ELSEVIER

Contents lists available at ScienceDirect

Remote Sensing of Environment

journal homepage: www.elsevier.com/locate/rse



Mitigating the black-soil problem in the reflectance-to-fluorescence (R2F) relationship: A soil-adjusted reflectance-based approach for downscaling SIF

Peiqi Yang ^{a,b,c,*}, Zhigang Liu ^d, Dalei Han ^{a,b,c}, Runfei Zhang ^{a,b,c}, Bastian Siegmann ^{e,k}, Jing Liu ^{a,b,c}, Huarong Zhao ^{f,g}, Uwe Rascher ^{e,l}, Jing M. Chen ^{h,i,j}, Christiaan van der Tol ^k

- ^a State Key Laboratory of Climate System Prediction and Risk Management, Nanjing, China
- ^b Key Laboratory of Virtual Geographic Environment, Ministry of Education, Nanjing Normal University, Nanjing, China
- c Jiangsu Center for Collaborative Innovation in Geographical Information Resource Development and Application, Nanjing, China
- d State Key Laboratory of Remote Sensing and Digital Earth, Faculty of Geographical Science, Beijing Normal University, Beijing 100875, China
- e Institute of Bio- and Geosciences, IBG-2: Plant Sciences, Forschungszentrum Jülich GmbH, Wilhelm-Johnen-Straße, 52428 Jülich, Germany
- f Chinese Academy of Meteorological Sciences, Beijing 100081, China
- g Hebei Gucheng Agricultural Meteorology National Observation and Research Station, Baoding 072656, China
- h School of Geographical Sciences, Fujian Normal University, Fuzhou, China,
- ⁱ Key Laboratory of Humid Subtropical Eco-Geographical Process, Ministry of Education, Fujian Normal University, Fuzhou, China,
- ^j Department of Geography and Planning, University of Toronto, Toronto, Canada
- k Faculty of Geo-Information Science and Earth Observation (ITC), University of Twente, P.O. Box 217, Enschede 7500 AE, the Netherlands
- ¹ University of Bonn, Faculty of Agricultural, Nutritional and Engineering Sciences, Institute of Crop Science and Resource Conservation, Karlrobert-Kreiten-Strasse 13, 53115 Bonn, Germany

ARTICLE INFO

Edited by: Marie Weiss

Keywords:
Solar-induced chlorophyll fluorescence
Fluorescence escape ratio
Soil effects
Total emitted SIF
Structural and angular correction

ABSTRACT

Solar-induced chlorophyll fluorescence (SIF) is an effective probe for photosynthesis, but this remote sensing signal is affected by multiple factors, including radiation intensity, canopy structure, sun-observer geometry, and leaf physiological status. The complex interplay among these factors causes substantial discrepancies among topof-canopy (TOC) SIF, leaf-level average SIF and actual photosynthetic activity. Downscaling TOC SIF to the leaflevel and decoupling structural and physiological information remain major challenges in the use of SIF signals for remote sensing of photosynthesis. To address these challenges, the R2F (reflectance-to-fluorescence) theory was developed, grounded in the similarity in radiative transfer processes governing SIF and reflectance. This theory establishes a physical relationship between near-infrared reflectance (R_{nir}) and the far-red SIF scattering coefficient (σ_F). On this basis, SIF signals can be scaled from the canopy to the leaf level by normalizing σ_F , estimated from reflectance as $\sigma_F = R_{nir}/i_0$, where i_0 denotes canopy interceptance. However, the original R2F formulation assumes a non-reflective soil. This simplification breaks down in sparse canopies, where soil contributions are non-negligible—an issue referred to as the "black-soil problem". Soil enhances both R_{nir} and σ_F , distorting their intrinsic relationship. In this study, we show that soil effects manifest through two main mechanisms: (1) direct soil reflection, which significantly increases R_{nir} but has minimal impact on σ_F , and (2) soil-vegetation multiple scattering, which affects both R_{nir} and σ_F but tends to have compensatory effects. Consequently, the dominant source of bias in the original R2F relationship is direct soil reflection that contributes to R_{nir} —a mechanism that had not been explicitly isolated in previous studies. This finding allows us to narrow down the "black-soil problem" in the R2F framework to the specific impact of soil single scattering on R_{nir} . To mitigate this bias, we propose a soil-adjusted R2F (saR2F) method, which estimates the direct soil contribution of R_{nir} using TOC red and blue reflectance. Correcting R_{nir} for the direct soil reflection results in a robust relationship between σ_F and soil-adjusted R_{nir} (saR_{nir}), notably $\sigma_F = saR_{nir}/i_0$.

We evaluated the saR2F relationship using one field and two simulated datasets. In the field study, saR2F improved the estimation of σ_F from TOC reflectance, with R² increasing ranging from 0.21 to 0.31 compared to

^{*} Corresponding author at: State Key Laboratory of Climate System Prediction and Risk Management, Nanjing, China. *E-mail address*: p.yang@njnu.edu.cn (P. Yang).

the original R2F. In the two simulations, saR2F consistently outperformed the original R2F, especially under sparse canopy conditions. We also compared saR2F with NDVI-based (NIRv) and FCVI-based R2F approaches. In the available field observations collected under specific conditions (i.e., varying viewing azimuth angles), the three approaches showed similar performance and were better than the original R2F in explaining the viewing-angle dependence of σ_F . However, across the broader range of simulated scenarios and for estimating the exact σ_F , saR2F demonstrated better stability than NIRv and FCVI-based R2F methods. The NIRv-based and FCVI-based R2F methods yielded relatively low RMSE (0.092 and 0.075, respectively) but weak explanatory power, with R² values below 0.41 for canopies with LAI < 3. In contrast, saR2F achieved a much stronger relationship (R² = 0.80) and a low RMSE of 0.044. Furthermore, compared to the NIRv or FCVI-based approaches for R2F corrections, saR2F offers a more physically plausible and interpretable solution that can be applied to angular correction and total SIF estimation. The effective mitigation of the black-soil problem facilitates interpretation of raw SIF observations and enhances the monitoring of photosynthetic activity using SIF.

1. Introduction

Solar-induced chlorophyll fluorescence (SIF) emitted by plants during photosynthesis has been explored as a proxy of actual photosynthesis (Baker, 2008; Mohammed et al., 2019b). Remote sensing of SIF by hyperspectral sensors provides means to monitor photosynthetic activity from space. However, top-of-canopy (TOC) SIF is influenced not only by leaf-level physiological processes directly related to photosynthesis, but also by factors such as soil background, canopy structure, and sun-observer geometry. These non-physiological influences complicate the interpretation of TOC SIF and highlight the need for correction or decoupling strategies.

The effects of various factors on TOC SIF observations are summarized into three key processes according to the light use efficiency (LUE) model (Mohammed et al., 2019b): i) the absorption of photosynthetically active radiation (PAR) by vegetation canopies, ii) the emission of fluorescence by photosystems, and iii) the scattering of SIF by soil and leaves after being emitted by photosystems. The impacts of these processes are quantified by fraction of absorbed PAR (fPAR), fluorescence emission efficiency (Φ_F), and scattering coefficient of the emitted SIF (σ_F), respectively (Porcar-Castell et al., 2014; Yang and van der Tol, 2018). Therefore, TOC observed SIF is expressed as

$$SIF = PAR \times fPAR \times \Phi_F \times \sigma_F \tag{1}$$

Vegetation canopy structure, leaf physiology, soil and sun-observer geometry affect TOC SIF via fPAR, Φ_F and σ_F . Among these three variables, fPAR is commonly used in the field of remote sensing of vegetation and ecological studies. In contrast, σ_F and Φ_F are unique variables used in SIF-related studies. The variable σ_F , describing the ratio of TOC directional SIF to total SIF emitted by photosystems, determines the angular variation in SIF, and affects the relationship between TOC SIF and gross primary productivity (GPP).

In a previous study, we established the link between the scattering coefficient of far-red SIF σ_F (also known as the escape probability of total emitted SIF, f_{esc}) and near-infrared (NIR) reflectance R_{nir} at wavelengths close to the far-red SIF retrievals (e.g., around 740-780 nm), by comparing their respective radiative transfer processes (Yang and van der Tol, 2018). We found that for dense vegetation canopies, or for canopies situated above a non-reflecting soil surface, σ_F was proportional to R_{nir} and to the reciprocal of canopy interceptance (i_0) , i.e., $\sigma_F =$ R_{nir}/i_0 . This relationship is based on the physical principle that, for photons of the same frequency, their subsequent interactions within the canopy-such as scattering, absorption, or escape-are independent of whether the photons originate from leaf scattering (contributing to R_{nir}) or from leaf fluorescence emission (contributing to SIF). The simple $R_{nir} - \sigma_F$ relationship is theoretically well-supported by multiple radiative transfer theories including the four-stream theory, the successive order of scattering theory, and the spectral invariant theory, as demonstrated in Yang and van der Tol (2018), and summarized in Section 2.1 of this study.

The relationship between R_{nir} and σ_F , hereafter referred to as the R2F (reflectance-to-fluorescence) relationship, has gained significant

attention for its role in quantifying the impact of scattering and reabsorption on TOC far-red SIF. It is crucial for estimating the total emitted SIF from vegetation canopies and correcting for the angular effects on SIF, both of which are important for improving GPP estimation (Hao et al., 2021b; Krämer et al., 2025; Li et al., 2018; Siegmann et al., 2021). For example, Lu et al. (2020) applied the R2F relationship in a deciduous-broadleaf-forest ecosystem to estimate the total canopyemitted SIF. They found field-measured GPP had a stronger correlation with the estimated total SIF than TOC SIF, with R² increasing from 0.51 to 0.64. Liu et al. (2019) used the R2F relationship to downscale airborne TOC SIF observations to the photosystem level. Their findings revealed an enhanced relationship between SIF and absorbed PAR (APAR) after SIF downscaling. The R2F relationship also illustrates that far-red SIF and R_{nir} exhibit similar patterns of variation, often showing bowl-shaped or dome-shaped distributions as the viewing angle shifts from backward to forward scattering directions (He et al., 2017; Joiner et al., 2020; Liu et al., 2016). According to this similarity, various methods that incorporate multiple angular observations of TOC reflectance have been developed to mitigate directional effects on TOC SIF for improving GPP estimation (Zhang et al., 2020b).

However, practical applications of the R2F relationship still face at least two noteworthy challenges (Mohammed et al., 2019b; Yang et al., 2020). First, the estimation of σ_F from R_{nir} needs the structural variable i_0 , which is not always available reliably. Second, the theoretical relationship between σ_F and R_{nir} is formulated by assuming a non-reflective soil beneath the vegetation canopy where soil effects are disregarded. Consequently, this relationship becomes less reliable in sparse canopies where the contribution of soil cannot be ignored.

Regarding canopy interceptance (i₀), researchers have sought to characterize its spatiotemporal variation using the canopy structural parameters. The variable i_0 describes the probability that the incident photons will interact with leaves rather than going through the canopy via gaps (Smolander and Stenberg, 2005; Stenberg et al., 2016). It is closely linked with canopy gap fraction, which can be estimated by using canopy structural properties, such as leaf area index (LAI) and clumping index according to Beer's law (Stenberg and Manninen, 2015). For instance, Lu et al. (2020) estimated the seasonal variations in i_0 by using the field measurements of LAI, and calculated σ_F and total SIF emitted by canopies. Zhang et al. (2020a, 2019) estimated i_0 at the global scale by using MODIS remote sensing products of LAI and clumping index. They further applied the R2F relationship and derived the total SIF from TROPOMI. Zeng et al. (2019) proposed to approximate i_0 using fPAR products, which are generated from TOC reflectance spectra. Although these approaches remain questionable given the inherent uncertainties in LAI and fPAR estimation itself, they are still widely used as practical proxies for estimating i₀ (Bendig et al., 2025; Yang et al., 2020).

In comparison to the amount of research on the estimation of canopy interceptance, the investigation of the soil effects has been relatively limited. A straightforward approach is to apply a threshold to exclude cases with pronounced soil effects, for example, the areas with low vegetation coverage. Beyond simple thresholding, NDVI, as an indicator of the fraction of vegetation coverage (FVC), has been used to mitigate

the soil effects on the R2F relationship. For example, Badgley et al. (2017) introduced NIRv as the product of R_{nir} and NDVI, and reported that NIRv, TOC SIF and GPP were strongly correlated via the vegetation coverage at the global scale. Researchers suggest that NIRv accounts for R_{nir} contributed by vegetation, and thus can be used to address the soil effects on the R2F relationship (Bendig et al., 2025; Hao et al., 2021b; Hao et al., 2021a; Zeng et al., 2019). This method leverages the negative correlation between NDVI and soil interference, as NDVI is inversely related to the fraction of exposed soil and thus to the soil's contribution to R_{nir} (Wan et al., 2024). Hence, it is expected that the inclusion of NDVI in the R2F relationship leads to an improvement in estimated σ_F compared to the original R2F-based approach (i.e., $\sigma_F = R_{nir} \times NDVI/i_0$ vs. $\sigma_F = R_{nir}/i_0$). However, relying on NDVI in a semi-empirical approach to remove soil effects on vegetation NIR reflectance may not produce a reasonable soil-adjusted R2F relationship. This is because soil influences not only vegetation reflectance but also σ_F . The soil effects on σ_F are often not explicitly addressed in the NDVI-based approaches. Furthermore, NDVI is not always a reliable surrogate for FVC, and FVC alone cannot fully account for soil-induced variability in R_{nir} . This is because soil effects also depend on spectral variability in soil reflectance that is independent of FVC. Therefore, relying solely on NDVI to correct soil effects may not yield a physically consistent or accurate soiladjusted R2F relationship.

In addition to NDVI, the fluorescence correction vegetation index (FCVI) is also used to estimate σ_F as FCVI/fPAR (Merrick et al., 2021; Siegmann et al., 2021). Yang et al. (2020) demonstrated that although it is difficult to estimate fPAR and σ_F individually by using just TOC reflectance, their product can be well approximated by a reflectance index, which is FCVI. FCVI is given as the difference of R_{nir} and broadband visible (VIS, from 400 to 700 nm) reflectance acquired under identical sun-canopy-observer geometry of the SIF measurements. Several studies have found that estimating σ_F using FCVI (i.e., σ_F = FCVI/fPAR) performs reasonably well even for sparse canopies (Bendig et al., 2025; Siegmann et al., 2021). This may be because the effects of soil on both FCVI and fPAR tend to offset each other. Nevertheless, the black-soil problem is not explicitly addressed in the development of FCVI, and its effectiveness in mitigating soil effects remains unclear.

Other more physically-based approaches have been developed to disentangle vegetation and soil contributions to canopy reflectance, including spectral unmixing techniques and radiative transfer modeling. For example, the NIRvH method estimates the R_{nir} of vegetation by decomposing hyperspectral signals, offering a way to minimize soil contributions (Bendig et al., 2025; Zeng et al., 2021). This method is based on the assumption of a linear mixture of soil and vegetation reflectance. However, when comparing the original NIRv and the more recent NIRvH approaches, a potential source of confusion arises. The original motivation for introducing NIRv was to account for soil background effects associated with R_{nir} . Yet in NIRvH, an additional layer of soil correction is applied on top of NIRv.

Despite the practical success of both NDVI-based and unmixingbased correction strategies, the theoretical underpinnings of each remain insufficiently clarified. This ambiguity makes it difficult to interpret the reliability and generalizability of these methods. This is especially true for SIF-related studies, where quantities such as σ_F or total emitted SIF are nearly impossible to measure directly in the field. As a result, we must rely on clear and well-founded theoretical developments to guide interpretation and methodological advances. Therefore, regardless of the correction strategy employed, a critical prerequisite for improving the performance of R2F (i.e., the R_{nir} - σ_F relationship) is a clear understanding of how soil influences this relationship. Identifying the specific mechanisms-whether direct soil reflection or multiple scattering pathways—that affect both R_{nir} and σ_F is essential for developing targeted and physically meaningful corrections. Building on this understanding, appropriate correction strategies can then be devised to address the specific soil-induced effects.

In this study, we present a theoretical analysis of the impact of soil on

TOC NIR reflectance, the scattering coefficient of far-red SIF, and their relationship. Further, we propose a way to account for the soil effects, and revise the R2F relationship to estimate the scattering coefficient of far-red SIF in sparse canopies. Field and simulated datasets are used to evaluate the performance of the soil-adjusted R2F (saR2F) relationship in estimating σ_F or correcting viewing-angle effects of TOC SIF.

2. Theory

2.1. A short review of the R2F relationship for black-soil canopies

The original R2F relationship is expressed as a simple function

$$\sigma_F^0 = \frac{\pi F_{toc}}{F_{rot}} = \frac{R_{nir}^0}{\hat{t}_0} \tag{2}$$

where F_{toc} is TOC SIF and F_{tot} total emitted SIF. R_{nir} refers to NIR reflectance at wavelengths close to those used for far-red SIF in remote sensing applications. The superscripts '0' indicate that the relationship holds when soil reflectance is zero (i.e., a black soil condition). Note that the superscript is applied to both σ_F and R_{nir} , as soil affects not only canopy reflectance but also the scattering of SIF—an influence that is often not considered.

The R2F relationship is based on the similarity in radiative transfer of the intercepted incident flux and the emitted SIF flux, which result in TOC NIR reflectance and SIF signals, respectively. A conceptual figure is provided to illustrate this relationship (Fig. 1). In canopies with black soil, the probability that the emitted SIF are scattered into the direction of the observer is denoted as σ_F^0 , which corresponds to the chance of fluxes transfer from F1 to F2 in Fig. 1a. Analogously, the probability that incoming solar photons are intercepted and scattered into the same direction is represented by R_{nir}^0 , corresponding to the probability of flux transfer from R0, R1 to R2 in Fig. 1a. Note both multiple scattering among leaves and single scattering are included in the paths of R1 to R2 and F1 to F2. For a more complete derivation, please refer to Yang and van der Tol (2018).

Once incident photons from the top of canopy are intercepted with probability i_0 , and subsequently scattered with probability ω_{nir} (i.e., the transition from R0 to R1 in Fig. 1a), their subsequent interactions with the vegetation canopy follow the same radiative transfer processes as the emitted SIF photons at the same wavelength. In other words, the probability of a photon transferring from R1 to R2 is identical to the probability of a photon transferring from F1 to F2. Therefore, the canopy reflectance R_{nir}^0 , which describes the radiative transfer from R0 to R2, is determined by the joint probability of the photon path from R0 to R1 (with probability $i_0 \times \omega_{nir}$), and from R1 to R2 (with probability σ_F^0): $R_{nir}^0 = i_0 \times \omega_{nir} \times \sigma_F^0$. Given that leaf albedo in the NIR region ω_{nir} is typically close to 1, we obtain the relationship shown in Eq. 2.

2.2. Soil effects on the R2F relationship

When black soil is replaced by a reflective (non-black) soil, both σ_F and R_{nir} increase due to the enhanced probability that photons scattered by leaves are further redirected into the observer's direction by the soil surface. This additional contribution from the soil is depicted by the dashed lines in Fig. 1b. Assuming an unchanged vegetation layer, increasing soil reflectance (R_{soil}) generally leads to concurrent increases in both σ_F and R_{nir} . However, the soil-induced changes in σ_F and R_{nir} are not necessarily proportional. This discrepancy implies that the original relationship $\sigma_F = \frac{R_{nir}}{i_0}$, which holds true under black-soil conditions, may no longer be valid in the presence of non-black soils.

Soil enhances TOC NIR reflectance through two main mechanisms: (i) directly reflecting incoming solar radiation toward the sensor, following the path SR4 \rightarrow SR5 \rightarrow SR6 in Fig. 1b, and (ii) reflecting radiation scattered by leaves and further redirecting it toward the sensor

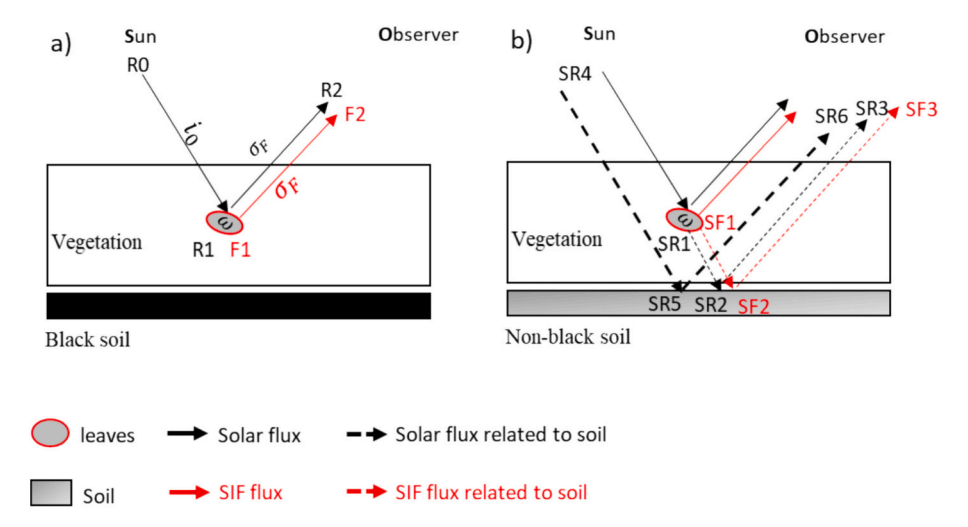


Fig. 1. Diagram illustrating the radiative transfer of incident solar fluxes (black lines) and emitted SIF fluxes (red lines) for (a) black-soil canopies and (b) non-black-soil canopies. The text notations in the diagram—'R', 'F', 'SR', and 'SF'—represent photon positions associated with reflectance (R), SIF (F), reflectance contributed by soil (SR), and SIF contributed by soil (SF), respectively. The notations on the arrowed lines indicate the probability of flux transfer between different positions. (For interpretation of the references to colour in this figure legend, the reader is referred to the web version of this article.)

via SR1 \rightarrow SR2 \rightarrow SR3, including multiple scattering between soil and leaves. In contrast, soil affects the scattering coefficient of emitted farred SIF primarily by reflecting SIF radiation emitted by leaves back into the canopy, thereby increasing the observed canopy SIF signals, as illustrated by the path SF1 \rightarrow SF2 \rightarrow SF3 in Fig. 1b. Owing to the similarity of radiative transfer at the same wavelength, the probability of photon transfer along SR1 \rightarrow SR2 \rightarrow SR3 is identical to that along SF1 \rightarrow SF2 \rightarrow SF3. The key distinction is the additional contribution of direct solar radiation to R_{nir} through SR4 \rightarrow SR5 \rightarrow SR6, a mechanism that does not apply to SIF, since SIF originates within the canopy rather than from solar input.

It is important to note that while soil can enhance total SIF emission by increasing the PAR absorbed by the vegetation canopy, this effect does not directly influence the scattering coefficient of SIF and thus does not affect the R2F relationship. Beyond the conceptual and pathway-based analysis presented in Fig. 1, we further employed the four-stream radiative transfer theory to quantitatively model the influence of soil on both σ_F and R_{nir} , and to assess its impact on the validity of the R2F relationship. The detailed mathematical derivation and model formulation are provided in Appendix A.

2.3. Soil adjustment of the R2F relationship

To revise the R2F relationship to account for soil effects, it is necessary to remove the contribution of direct soil reflection (denoted as ρ_{nir}^{s1}) from the TOC NIR reflectance. This leads to the soil-adjusted R2F relationship:

$$\sigma_F = \frac{R_{nir} - \rho_{nir}^{s1}}{i_0} \tag{3}$$

This formulation is consistent with the original R2F relationship for black-soil canopies, as presented in Eq. 2. Specifically, when the soil reflectance is zero, ρ_{nir}^{s1} becomes zero, and Eq. 3 simplifies to Eq. 2. For dense canopies, where the underlying soil is largely masked by the vegetation, ρ_{nir}^{s1} remains small and the difference between the adjusted and unadjusted relationships is negligible. However, for sparse canopies with bright soils, where ρ_{nir}^{s1} can be substantial, this correction becomes essential to accurately represent the relationship between σ_F and R_{nir} .

Yang et al. (2025) develop three approaches to estimate the direct soil reflection component ρ_{nir}^{s1} , based on distinct spectral signatures of soil and vegetation. The term ρ_{nir}^{s1} , is calculated as the product of the probability that the soil is both sunlit and visible to the sensor (P_{so}^{soil}) and

the soil reflectance in the NIR (R_{nir}^s). Two of the methods rely on known soil reflectance data: (1) a single-band approach using red reflectance (RBB), where P_{so}^{soil} is estimated as R_{675}/R_{675}^s , and (2) a two-band approach based on the spectral contrast between red and blue bands (TBB), where P_{so}^{soil} is estimated as $(R_{675}-R_{438})/(R_{675}^s-R_{438}^s)$. However, the applicability of these two methods is limited in practice due to their dependence on accurate soil reflectance measurements, which are not always readily available in heterogeneous or natural environments.

To address the limitation of requiring known soil reflectance, a third method was proposed that avoids this dependency by assuming a nearlinear spectral dependence of soil reflectance between 400 and 1000 nm (LAB). Under this assumption, the contribution of direct soil reflection to TOC reflectance increases linearly with wavelength, given that P_{so}^{soil} is spectrally independent.

$$\rho_{\lambda}^{s1} = P_{so}^{soil} \times (k_s \lambda + b_s) \tag{4}$$

For green vegetation, leaf albedo in the blue and red spectral regions is close to zero, meaning that TOC reflectance at these wavelengths primarily originates from direct soil reflection. Because chlorophyll exhibits maximum absorption near 438 nm and 675 nm, the TOC reflectance at these bands can be used to approximate the corresponding direct soil contributions:

$$\rho_{438}^{s1} = P_{so}^{soil} \times (438k_s + b_s) = R_{438} \tag{5a}$$

$$\rho_{675}^{s1} = P_{so}^{soil} \times (675k_s + b_s) = R_{675} \tag{5b}$$

where ρ_{λ}^{s1} represents the contribution of soil single scattering to TOC reflectance at wavelength λ in nanometers (nm); P_{so}^{soil} is the probability that the soil is illuminated by the sun and observed by the sensor; k_s and b_s are the slope and intercept of the linear fit between soil reflectance $R_s(\lambda)$ and wavelength λ in the range of 400 nm to 800 nm, respectively; R_{λ} is the TOC reflectance at wavelength λ . Therefore, the contribution of direct soil reflection to TOC NIR reflectance can be predicted from blue and red TOC reflectance through linear extrapolation by combining Eq. 4 and 5. For instance, at 770 nm, the direct soil reflection component can be estimated as:

$$\rho_{770}^{s1} = P_{s0}^{soil} \times (770k_s + b_s) = 1.40R_{675} - 0.40R_{438}$$
(6)

By substituting Eq. 6 into Eq. 3, we obtain a semi-empirical R2F formulation that corrects for soil effects without requiring prior knowledge of soil spectral properties.

$$\sigma_F = \frac{R_{770} - 1.40R_{675} + 0.40R_{438}}{i_0} \tag{7}$$

The saR2F relationship also aligns with the original R2F relationship for black-soil canopies in Eq. 2. When the soil reflectance is zero, the term $1.40R_{675}-0.40R_{438}$ becomes negligible, and Eq. 7 reduces to Eq. 2. It is important to note that TOC reflectance at 770 nm was used as an approximation for the true value at 760 nm. This is because remotely sensed apparent TOC reflectance at 760 nm is often overestimated due to fluorescence effects, which can distort the actual signal. For convenience, we refer to $R_{nir}-1.40R_{675}+0.40R_{438}$ as saR_{nir} (soil-adjusted R_{nir}) hereafter. For detailed descriptions of the soil correction methods and their evaluation, the readers are referred to Yang et al. (2025).

3. Evaluation

3.1. Evaluation with field multi-angle experiment

Due to the inherent challenges of directly measuring σ_F or F_{tot} in the field, direct validation of the methods in Table 1 using these quantities is often unfeasible. To address this limitation, we conducted a dedicated multi-angular field experiment, i.e., field measurements under fixed canopy structure and illumination conditions, with only the viewing angle varying. Under these controlled conditions, both F_{tot} and i_0 remain relatively constant, so the observed variation in F_{toc} proportionally reflects changes in σ_F :

$$\sigma_F \propto F_{toc}$$
 (8)

We assessed the methods listed in Table 1 by examining the correlation between F_{toc} and the numerator of each R2F formulation, including R_{nir} , saR_{nir} , NIRv and FCVI. We hypothesize that all four reflectance-based metrics should exhibit a positive correlation with F_{toc} , as their angular responses are expected to follow a similar directional pattern. Moreover, under conditions of low vegetation cover, saR_{nir} is expected to show a stronger correlation with F_{toc} than R_{nir} , owing to its enhanced ability to account for soil background effects.

3.1.1. Study site and experimental setup

Field experiments on winter wheat (*Triticum aestivum L.*) were conducted on March 16 and 21, 2025, in Gucheng, Baoding City, China (39.14455°N, 115.73785°E). The experimental plot has a size of 24 \times 12 m with an average elevation of 15.2 m above sea level. The site experiences a mean annual temperature of 12.1 °C and an average annual precipitation of 479.6 mm.

Wheat was sown on October 17, 2024, in north–south-oriented rows at a density of approximately 700,000 plants ${\rm ha}^{-1}$, corresponding to 6.8 rows per meter perpendicular to the row direction, with a 5-cm inter-

Table 1Formulae of the original R2F relationship, and the soil-adjusted R2F relationship to estimate the scattering of far-red SIF with NIR reflectance.

Labels	Formulae	References
Original R2F	$\sigma_F = rac{R_{nir}}{i_0}$	(Yang and van der Tol, 2018)
saR2F	$\sigma_F = \frac{R_{nir} - 1.40R_{675} + 0.40R_{438}}{i_0} =$	This study
	$\frac{saR_{nir}}{i_0}$	
NDVI-based R2F	$\sigma_F = rac{R_{nir} imes NDVI}{i_0} = rac{NIR_{ u}}{i_0}$	(Badgley et al., 2017; Zeng et al., 2019)
FCVI-based R2F	$\sigma_F = rac{FCVI}{i_0} = rac{R_{nir} - R_{vis}}{i_0}$	(Yang et al., 2020)

Note: R_{nir} refers to the reflectance at approximately 770 nm, consistent with the far-red SIF retrieval region. R_{vis} is the average reflectance over the 400–700 nm range. NDVI is calculated using the MODIS band configuration (Red: 620–670 nm; NIR: 841–876 nm).

row spacing. During the measurement period, the canopy had an average height of $\sim \! 12$ cm and exhibited partial closure, with clearly visible row structure and exposed bare soil between rows. We deliberately selected a period with relatively low vegetation coverage for analysis, as higher coverage tends to reduce the variability of observed SIF across different viewing azimuth angles. Under such conditions, the differences in SIF signals observed from different viewing angles become less pronounced, making it difficult to evaluate the performance of the saR2F relationship through correlation analyses among relevant variables, e.g., F_{toc} from different viewing angles and R_{nii} .

3.1.2. Instrumentation and measurement protocol

The canopy observation system comprised a computer-controlled pan-tilt unit (PTU-E46, FLIR Systems, USA) mounted on a 2 m-high platform, integrating a dual-spectrometer measurement system. The PTU, driven by a stepper motor and rotating platform, executed software-controlled rotations in both azimuth and elevation to enable automated, multi-angular measurements. Two spectrometer probes, each with a 25° field of view, were affixed to the PTU to simultaneously measure canopy reflectance and SIF. Reflectance data were collected using an HR2000 spectrometer (Ocean Insight Inc., Dunedin, FL, USA), which covers the 300–1200 nm spectral range with a resolution of 3 nm. These data were used to compute the reflectance-based terms in the R2F formulations. For SIF retrieval, a QE65Pro spectrometer (Ocean Insight Inc., Dunedin, FL, USA) was employed, offering a higher spectral resolution of 0.7 nm over the 640-800 nm range with 1036 channels. Far-red SIF was calculated with the spectral fitting method (SFM, Cogliati et al., 2019). Further details about the measurement system can be found in Yang et al. (2025).

Data collection was conducted near solar noon (11:30–13:30 local time) under stable illumination conditions. During the measurement period, the solar zenith angle (SZA) varied from 38° to 43°. Angular sampling followed a structured protocol: each observation sequence comprised measurements at 13 predefined azimuth angles (ranging from 60° to 300° in 20° increments), with zenith angles dynamically adjusted to match the real-time SZA, capped at a maximum of 40°. This strategy yielded a sector-shaped observation footprint with an approximate radius of 2.6 m (see Fig. 2). Each observation sequence lasted \sim 6 min, a duration short enough to assume negligible variation in both total incoming radiation and the fraction of intercepted radiation (i_0), and thus total emitted SIF (F_{tot}). One complete observation sequence was conducted every 30 min, resulting in four datasets collected per day during the selected time window.

Supporting biophysical parameters were collected to characterize canopy structure. LAI was quantified using a destructive sampling method. To calculate LAI, we first measured the total single-sided leaf area (SLA) from wheat leaves sampled along a 0.3-m row segment. The leaf area per unit row length (LA, in $\rm m^2 \cdot m^{-1}$) was then calculated as: LA = SLA/0.3. To upscale to plot-level LAI, we considered the number of rows per meter in the cross-row direction (6.8 rows·m $^{-1}$) and the total plot dimensions (M \times N, in meters), where M is the row length and N is the cross-row width. The leaf area per row is LA \times M, and the number of rows in the plot is N \times 6.8. Hence, the total leaf area over the entire plot is given by: LA \times M \times 6.8 \times N. LAI was calculated by normalizing the total leaf area by the ground area (M \times N): SLA/0.3 \times 6.8. This simplification assumes uniform row spacing and plant distribution across the plot. The LAI values of the wheat canopy were 0.71 and 0.89 on March 16 and 21, 2025, respectively.

3.2. Evaluation with the SCOPE model

Because accurate field measurements of σ_F or F_{tot} are difficult to obtain, we employed virtual scenarios and radiative transfer models (RTMs) to directly evaluate the proposed soil correction methods. RTMs simulate the values of σ_F , F_{tot} , i_0 and canopy reflectance based on physical principles, enabling direct testing of the relationships outlined

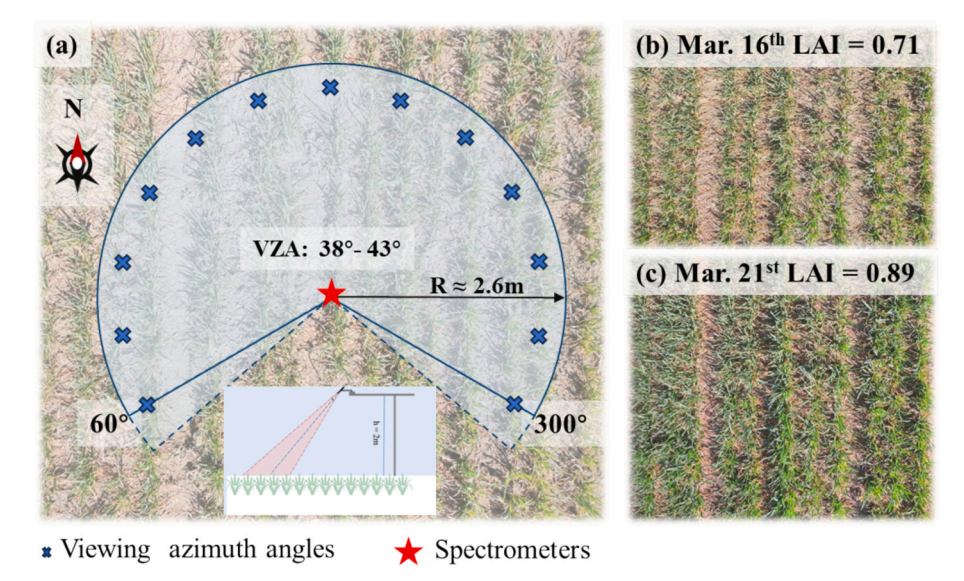


Fig. 2. Setup for multi-angular observations of SIF and reflectance (a). Nadir-view RGB images of the wheat canopy taken on March 16 and 21, 2025, are shown in (b) and (c), respectively. The blue cross symbols indicate the predefined viewing azimuth angles (VAA). (For interpretation of the references to colour in this figure legend, the reader is referred to the web version of this article.)

in Table 1.

3.2.1. The SCOPE model

SCOPE (Soil-Canopy Observation of Photochemistry and Energy fluxes, Van Der Tol et al., 2009; Yang et al., 2021) is one of the most widely used models for analyzing the factors and processes that govern TOC SIF. In SCOPE, vegetation is typically represented as a single homogeneous layer of leaves situated above a soil surface, with leaf orientation allowed to vary within the canopy. The model integrates a leaf-level RTM (Fluspect), multiple canopy-level RTMs, and an energy balance module. At the leaf level, Fluspect simulates leaf reflectance, transmittance, and both forward and backward fluorescence emission (Vilfan et al., 2018). At the canopy scale, RTMo and RTMf—two radiative transfer models based on the SAIL framework (Verhoef, 1984)—simulate the transfer of incident radiation and the emission of fluorescence, respectively. The model is publicly available in an online repository: https://github.com/Christiaanyandertol/SCOPE.

SCOPE generates all the other necessary variables for evaluating the original R2F, soil-adjusted R2F (saR2F), NDVI-based and FCVI-based R2F relationships. These variables include TOC spectral reflectance $R(\lambda)$, canopy interceptance i_0 and the true scattering coefficient of farred SIF (σ_F) at 760 nm. Among these variables, TOC reflectance is a direct output of SCOPE, while σ_F and i_0 are intermediate variables derived within the model. The scattering coefficient σ_F is computed as the ratio of TOC SIF and canopy total emitted SIF, both simulated by RTMf. The canopy interceptance i_0 is calculated in SCOPE as $1-\exp(-kL)$, where k is the extinction coefficient and L is the canopy LAI, assuming direct illumination. The extinction coefficient k depends on the solar zenith angle and the leaf inclination distribution. This formulation is consistent with the definition of canopy interceptance used in Smolander and Stenberg (2005).

3.2.2. Synthetic scenarios

The first set of synthetic scenarios aimed at testing the overall performance of the R2F relationships listed in Table 1. A wide range of synthetic scenarios were generated to examine the soil effects on R_{nir} and σ_F , and to evaluate the performance of the original R2F, saR2F, NDVI-based and FCVI-based R2F relationships in estimating σ_F . These scenarios covered all possible combinations of soil reflectance, leaf biophysical properties, canopy structural parameters, and sun-observer geometry listed in Table 2. The setup largely followed Yang and van der

 Table 2

 Summary of SCOPE inputs applied for the generation of the dataset.

Variables	Definitions	Units	Values
Cab	Chlorophyll $a+b$ content	$\mu {\rm g~cm}^{-2}$	10, 20, 30,40, 50, 60,70 or 80
LAI	Leaf area index	$_{\rm m}2_{\rm m}-2$	0.5, 1, 2, 3, 4, 5, 6, 7 or 8
LAD	Leaf angle distribution	-	spherical, planophile, or erectophile
θ_s	Solar zenith angle	degree	30, 45 or 60
θ_o	Viewing zenith angle	degree	0, 20, 40 or 60
R^S	Soil reflectance	-	0.1, 0.2, 0.3 at 760 nm

Tol (2018), but with an expanded range. Specifically, LAI varied from 0.5 to 8 m² m⁻², leaf chlorophyll content from 10 to 80 $\mu g \cdot cm^{-2}$. Leaf angle distribution (LAD) types included spherical, planophile to erectophile. Three different soil backgrounds were used, with NIR reflectance at 760 nm equaling 0.3, 0.2 and 0.1. The corresponding soil reflectance spectra, derived from field measurements, are available in the online GitHub repository. Solar zenith angles (θ_s) were set to 30, 45 or 60 degrees, and the viewing angles (θ_o) were set to 0, 20, 40 or 60 degrees. These variables were selected due to their known influence on canopy reflectance and SIF (Hinojo-Hinojo and Goulden, 2020), whereas other parameters—such as leaf water and dry matter content—were kept at the default values defined in SCOPE.

The second set of synthetic scenarios was designed to evaluate the performance of the R2F relationships listed in Table 1 in correcting for viewing-angle effects. This design mirrored the setup of the field experiment but explored a broader range of canopy LAI conditions and viewing zenith angles. The simulations comprised four groups, each representing a different canopy LAI, while keeping canopy LAD, soil background, and leaf optical properties constant. Specifically, a spherical LAD, a dry soil surface, and SCOPE default leaf biochemical parameters were applied. Within each group, observations were simulated at 2° intervals for both viewing zenith and azimuth angles, with a finer 1° interval in the hot spot direction to better capture angular effects. The solar zenith angle was fixed at 30° to maintain consistent illumination across scenarios and enable a systematic analysis of the impact of viewing geometry. For canopies with the same LAI, variations in viewing angle do not affect F_{tot} but do influence σ_F , thereby altering F_{toc} . Consequently, estimating σ_F using the R2F methods enables subsequent estimation of F_{tot} . By comparing the true and R2F-derived F_{tot} values

across different LAI levels, we assessed the accuracy and robustness of the various R2F-based approaches, and identify the most reliable formulation under varying canopy densities.

4. Results

4.1. Performance of the four R2F methods across synthetic scenarios

4.1.1. Overall performance of the four R2F methods

We evaluated the performance of four R2F methods across the first set of synthetic scenarios. Among them, soil-adjusted R2F (saR2F) shows the least sensitivity to LAI, whereas the original R2F relationship, which exhibits substantial errors in low LAI cases (LAI < 3; Fig. 3a vs. Fig. 3c). For dense canopies (LAI \ge 3), the original R2F relationship provides accurate estimates of σ_F , with a low RMSE of 0.040 and high R² of 0.817 (Fig. 3b). However, for sparse canopies (LAI < 3), particularly for LAI <

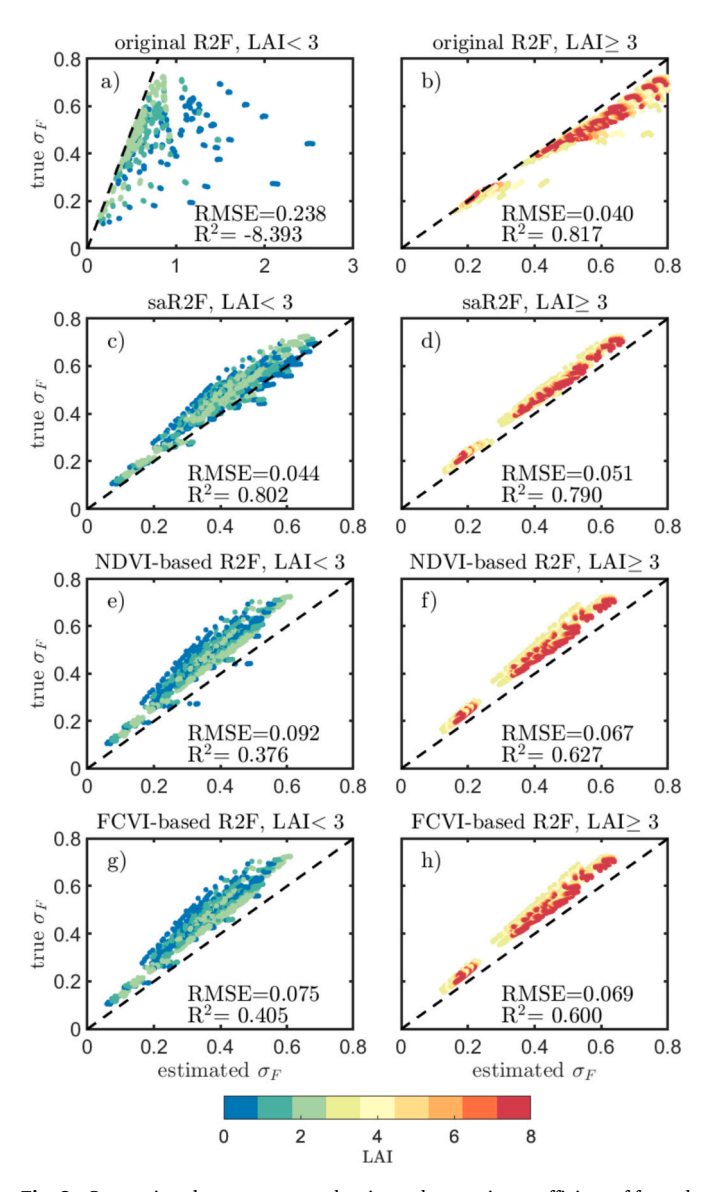


Fig. 3. Comparison between true and estimated scattering coefficient of far-red SIF (σ_F) using four R2F based methods: the original R2F, soil-adjusted R2F (saR2F), NDVI-based (NIRv) and FCVI-based R2F, under various non-black-soil scenarios. Left panels correspond to sparse canopies (LAI < 3); right panels correspond to dense canopies (LAI \geq 3). RMSE and R^2 values are shown in each panel, with R^2 computed based on the 1:1 (slope = 1) model. (For interpretation of the references to colour in this figure legend, the reader is referred to the web version of this article.)

1, it significantly overestimates σ_F —sometimes predicting values as high as 3. This leads to a much larger RMSE of 0.238 for low LAI cases, and a negative R^2 of -8.393 (Fig. 3a).

In contrast, the saR2F method maintains robust performance across canopy densities, with RMSEs substantially lower than the original R2F. Specifically, it achieves RMSEs of 0.044 for LAI < 3 and 0.051 for LAI \geq 3. The R^2 values using the 1-to-1 model are 0.802 and 0.790, respectively (Fig. 3c and d). These values indicate consistently accurate predictions and a strong 1:1 correspondence with true σ_F .

The NDVI-based and FCVI-based R2F methods also outperform the original R2F in sparse canopies. For LAI < 3, the FCVI-based and NDVI-based methods yields low RMSE of 0.075 and 0.092, respectively (Fig. 3e-3g). However, both methods exhibited low R² values under sparse conditions (R² = 0.405 for FCVI and 0.376 for NDVI), indicating that they failed to capture the variability in σ_F and tended to make overregularized predictions centered near the mean. In dense canopies (LAI \geq 3), the original R2F method remains the most accurate (RMSE = 0.040), followed by saR2F (0.051), NDVI-based (0.067), and FCVI-based (0.069). The predictions from the saR2F are more tightly along the 1:1 line than the NDVI-based and FCVI-based R2F methods.

Further comparing the three soil-adjusted R2F methods, we find that the saR2F method exhibits the most stable performance across all NDVI ranges, with relative errors generally within ± 35 % (Fig. 4). As NDVI increases, the error distribution becomes narrower. Specifically, when NDVI >0.8 (Fig. 4d), the errors for saR2F are tightly constrained between approximately -15 % and 0 %. In contrast, the NDVI-based R2F method systematically underestimates σ_F across all NDVI ranges, particularly evident when NDVI is below 0.6 (Fig. 4a and b), where the median errors approach -20 %. The FCVI-based R2F method shows intermediate performance: although it also tends to slightly underestimate σ_F , the errors are smaller and more symmetrically distributed compared to the NDVI-based method, especially when NDVI is higher than 0.6 (Fig. 4c and d). Overall, the performance of all three soil-adjusted R2F methods is better for the denser canopy (higher NDVI), but the saR2F consistently achieves the best accuracy and stability.

4.1.2. Performance of the four R2F methods for correcting viewing angle effects

In comparing the accuracy of four R2F methods for correcting viewing angle effects and obtaining F_{tot} , we find that all methods perform adequately when LAI \geq 3. However, for sparser canopies, the advantage of the soil-adjusted R2F (saR2F) method becomes increasingly evident (Fig. 5). For LAI = 0.5 (Fig. 5a), the original R2F method shows the largest error, with a median error of approximately 55 %. The NDVI-based and FCVI-based methods offer notable improvements, reducing the median error to around 25 % and 24 %, respectively. In contrast, the saR2F method yields the most accurate results, with median errors close to zero.

A similar pattern is observed at LAI = 1 (Fig. 5b): the original R2F method still produces a median error of about 38 %, while the NDVI-based and FCVI-based methods perform better, and the saR2F method once again achieves near-zero error. As LAI increases to 3 and 6 (Fig. 5c and d), the errors from the original R2F method markedly decrease, and all four methods provide reliable estimates, with median errors converging to around 10 %.

To assess how viewing geometry influences the performance of the R2F methods, we analyzed the relative errors as a function of viewing angle for a representative canopy with LAI = 0.5 (Fig. 6). The original R2F method exhibits the largest errors, with relative errors exceeding 60 % across most angles (Fig. 6a). In contrast, the saR2F method shows consistently low errors, generally remaining below 5 % regardless of viewing direction (Fig. 6b). The FCVI-based method performs moderately well, with errors above 30 % at narrow viewing angles, decreasing to below 10 % at viewing zenith angles greater than 60° (Fig. 6d). The NDVI-based method displays a similar trend, with errors above 30 % across most viewing angles, improving only at extreme off-nadir angles

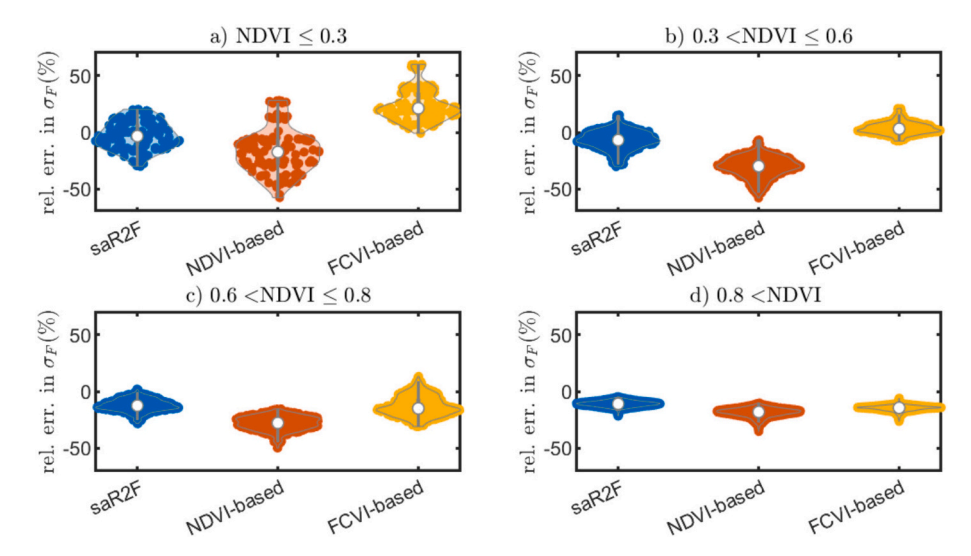


Fig. 4. Relative errors in the estimated scattering coefficient of far-red SIF (σ_F) using the soil-adjusted R2F (saR2F), NDVI-based (NIRv) and FCVI-based R2F relationships for various NDVI levels. (For interpretation of the references to colour in this figure legend, the reader is referred to the web version of this article.)

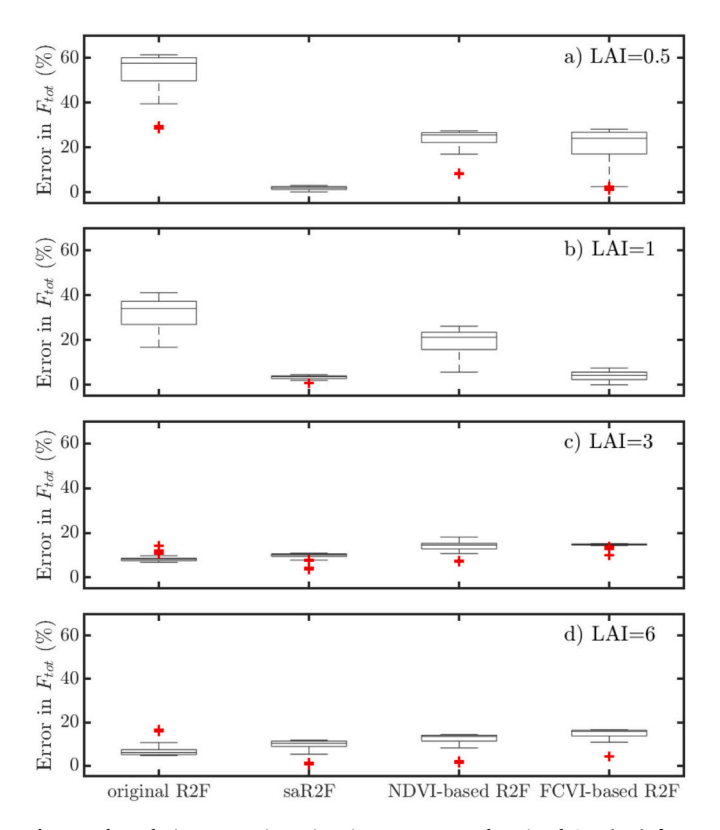


Fig. 5. The relative errors in estimating canopy total emitted SIF (F_{tot}) from TOC SIF (F_{toc}) observed at various viewing angles by using the original R2F, soil-adjusted R2F (saR2F), NDVI-based (NIRv) and FCVI-based R2F relationships across four LAI levels (0.5, 1, 3, and 6).

 $(>\!70^\circ).$ Overall, relative errors tend to decrease with increasing viewing zenith angle, as when viewing at these large angles the effect of the soil becomes again negligible.

4.2. Performance across multi-angle field SIF observations

When evaluating the performance of the four R2F methods using the field datasets by examining the correlation between R_{770} , saR_{770} , NIRv and FCVI and F_{toc} , we find that the three soil-adjusted methods consis-

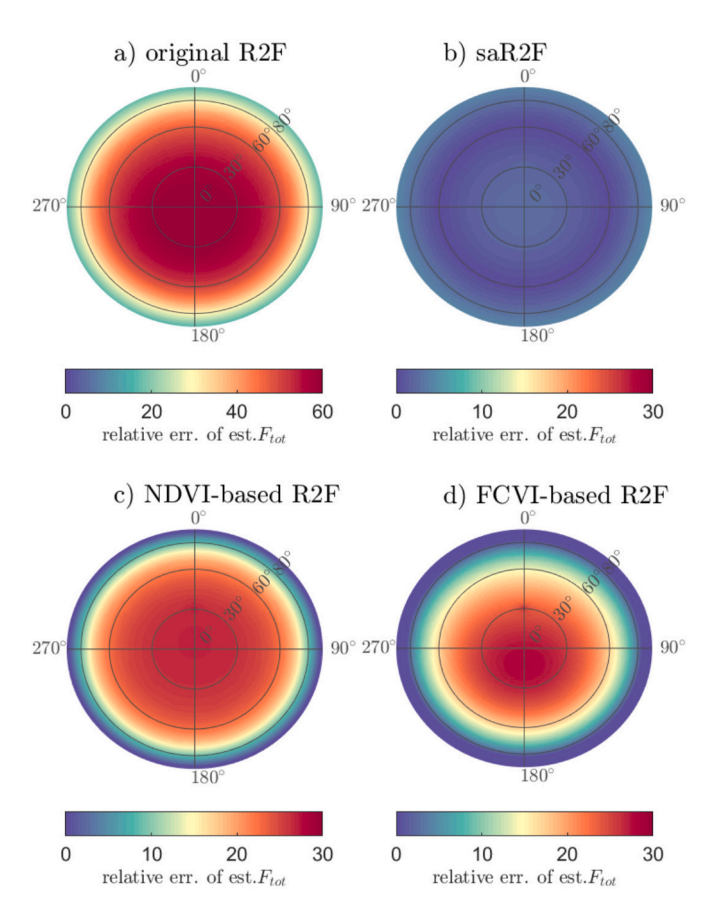


Fig. 6. The angular distribution of relative errors in estimating canopy total emitted SIF (F_{tot}) from TOC SIF (F_{toc}) by using the original R2F, soil-adjusted R2F (saR2F), NDVI-based (NIRv) and FCVI-based R2F relationships for a canopy with LAI of 0.5.

tently outperform the original R2F method. On March 16 (LAI = 0.71; Fig. 7a–d), the original R2F method shows the weakest performance, with correlation coefficients between R_{770} and F_{toc} ranging from 0.54 to 0.71. In contrast, the saR2F method achieves significantly higher correlations, improving by 0.21–0.31 over the original R2F. The NDVI- and FCVI-based methods also yield stronger correlations, exceeding the

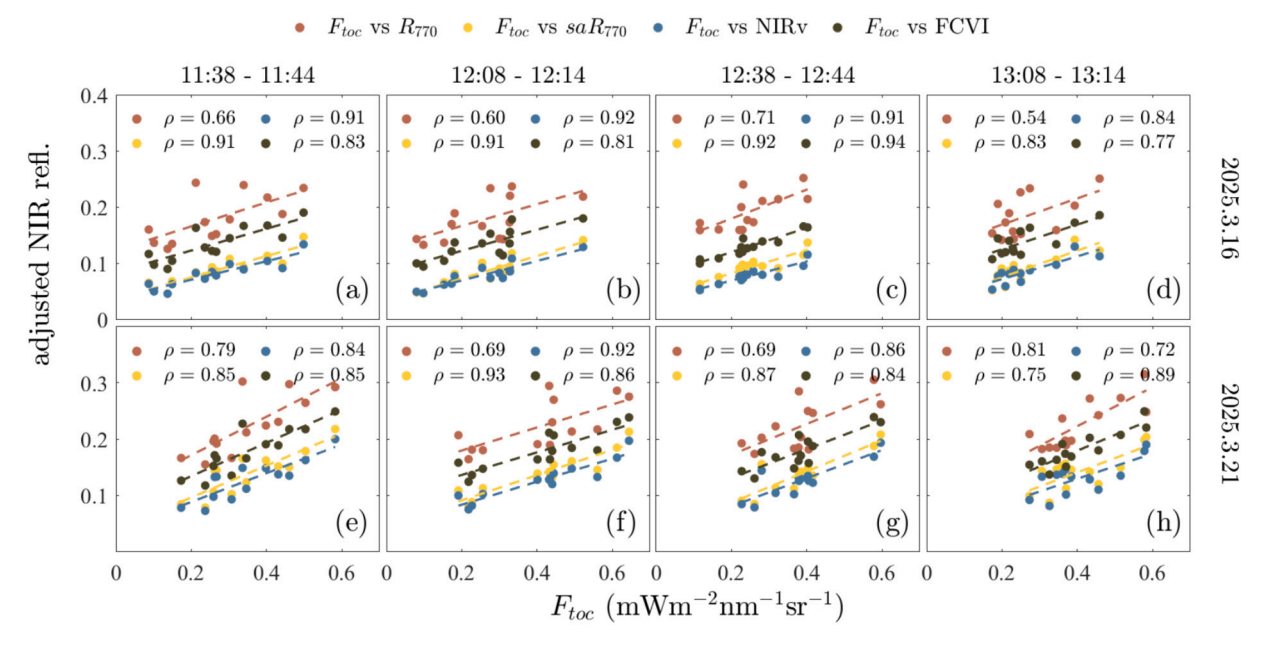


Fig. 7. Pearson correlation coefficients (ρ) among F_{toc} and R_{770} , saR_{770} , NIRv and FCVI. Panels (a) to (d) correspond to measurements on March 16, LAI = 0.71, while panels (e)–(h) correspond to March 21 (LAI = 0.89). Each panel represents one set of data collected within a short period under similar illumination but different viewing azimuth angles.

original R2F by 0.20-0.32 and 0.17-0.23, respectively.

When LAI is slightly higher (March 21, LAI = 0.89; Fig. 7e–h), the original R2F method shows moderate improvement compared to the correlation on March 16, with correlations rising to 0.69–0.81. Although the performance of the original R2F improves, the soil-adjusted methods still perform better. saR_{770} and F_{toc} maintain high correlation coefficients ranging from 0.75 to 0.93, while the correlations for NDVI-and FCVI-based methods range from 0.72 to 0.92 and 0.84 to 0.89, respectively.

The correlation between F_{toc} and R_{770} is relatively weak ($\rho=0.69\pm0.09$), indicating the limited reliability of the original R2F approach under varying geometric conditions (Table 3). In contrast, the three soil-adjusted R2F methods— saR_{770} , NIRv and FCVI—exhibit much stronger correlations with F_{toc} , with ρ values of 0.87 ± 0.06 , 0.87 ± 0.07 , and 0.85 ± 0.05 , respectively. Among the soil-adjusted indices, saR_{770} and NIRv are almost perfectly correlated ($\rho=0.99\pm0.00$), suggesting that they are nearly interchangeable in this dataset. FCVI also shows high consistency with both saR_{770} ($\rho=0.86\pm0.07$) and NIRv ($\rho=0.87\pm0.06$), highlighting the strong internal agreement among the three soil-adjusted approaches. These results collectively underscore the advantage of soil-adjusted methods over the original R2F in improving the stability and accuracy of F_{toc} estimation across different viewing geometries.

Table 3 Pearson correlation coefficients (mean \pm standard deviation) among F_{toc} and R_{770} , saR_{770} , NIRv and FCVI, based on eight groups of multi-angular observations collected under different viewing azimuth angles. The reported mean and standard deviation represent the statistics of the eight groups of measurements taken over two days, as shown in Fig. 7.

	F_{toc}	R ₇₇₀	saR ₇₇₀	NIRv	FCVI
F_{toc}	1.00				
R_{770}	0.69 ± 0.09	1.00			
saR ₇₇₀	0.87 ± 0.06	0.62 ± 0.14	1.00		
NIRv	0.87 ± 0.07	0.63 ± 0.13	0.99 ± 0.00	1.00	
FCVI	0.85 ± 0.05	0.93 ± 0.03	0.86 ± 0.07	0.87 ± 0.06	1.00

5. Discussion

5.1. Soil correction to the original R2F relationship

We extended the original R2F framework by explicitly addressing the black-soil assumption problem. We presented a theoretical analysis showing that although soil enhances both R_{nir} and σ_F , the impact of soil-vegetation multiple scattering on R_{nir} and σ_F tends to cancel out, and the dominant additional effects on the original R2F relationship stem from direct soil reflection on R_{nir} . The extra contribution of direct soil reflection aligns with the simulation results that the magnitude of the soil-induced enhancement of R_{nir} is greater than that of σ_F (see Appendix B). Based on this insight, we developed a saR2F relationship by incorporating TOC red and blue reflectance to estimate the direct soil reflection and correct it. This improved relationship allows a more accurate estimation of σ_F , especially in sparse canopies where the soil signal is strong.

Field and simulation experiments confirmed that the saR2F relationship outperforms the original R2F relationship, especially under low vegetation cover conditions (Figs. 3–7). When the canopy is sparse, the interception of incoming radiation is low. If soil reflectance is assumed to be zero, both R_{nir} and i_0 would be very small, and R_{nir}/i_0 would yield values comparable to σ_F . However, when the soil is reflective, R_{nir} becomes higher while i_0 remains small, leading to unrealistically large values of R_{nir}/i_0 and rendering it unreliable for estimating σ_F (e.g., blue dots in Fig. 3a). This phenomenon is consistent with the simulations reported by Zeng et al. (2019) and was recognized by Yang and van der Tol (2018) as the "black-soil background problem". After applying the soil correction, these outliers are largely eliminated, and the estimated σ_F falls within a physically reasonable range, especially for sparse canopies (Fig. 3b). We also observed that soil correction becomes increasingly necessary with decreasing vegetation LAI, as lower canopy coverage leads to greater exposure of soil, which biases the estimation of σ_F from uncorrected R_{nir} . By removing the direct soil contribution of R_{nir} , the correspondence between reflectance and σ_F is significantly improved.

The saR2F relationship also provides improved angular correction of TOC SIF using TOC reflectance, particularly when observing at different viewing zenith angles (Fig. 6). In dense canopies, changes in viewing

angle mainly affect the relative contributions of sunlit and shaded leaves to both reflectance and SIF. Due to the similarity in radiative transfer processes for R_{nir} and SIF within the vegetation layer, their directional effects are nearly identical, as supported by Liu et al. (2016), He et al. (2017) Joiner et al. (2020) and our results (Fig. 5c and d). However, in sparse canopies, changes in viewing angle not only alter the sunlit—shaded leaf ratio but also substantially affect the observed soil fraction. Soil directly reflects incoming radiation and enhances R_{nir} , but does not emit SIF. This distorts the relationship between R_{nir} and σ_F under the non-black soil condition, as shown in Figs. 5a, b, 6, and 7.

The observed systematic underestimation of σ_F (Fig. 3b-d) when using saR2F or related R2F-based approaches (e.g., NIRv and FCVI) can be attributed to several factors. First, the theoretical relationship between σ_F and R_{nir} is defined as $\sigma_F = R_{nir}/(i_0\omega_{nir})$ according to the original R2F framework, where ω_{nir} is the NIR leaf albedo (Yang and van der Tol, 2018). In practice, however, due to the difficulty in directly measuring leaf albedo, ω_{nir} is often assumed to be 1 for simplicity. While this assumption is generally acceptable, it leads to an underestimation of σ_F because actual ω_{nir} values are typically lower. Using more realistic ω_{nir} values (i.e., 0.95 or 0.9) in practical applications can help alleviate this bias. Second, the LAB soil correction method proposed by Yang et al. (2025), employed in our analysis, has been found to overestimate the direct soil contribution (see Fig. 8c in Yang et al., 2025), thereby contributing to the systematic underestimation of σ_F . Third, the R2F framework was proposed by assuming equivalence between leaf reflectance and transmittance. While this simplification may introduce

some bias, our earlier study showed that the effect of optical asymmetry does not cause a consistent offset (see Fig. 10B in Yang and van der Tol, 2018), which differs from the consistent underestimation of σ_F as shown in Fig. 2. Therefore, we conclude that the assumption of $\omega_{nir} = 1$ and potential overcorrection by the soil adjustment method are the primary sources of σ_F underestimation, and addressing these issues will be important for improving the accuracy of future R2F-based approaches.

5.2. The effectiveness and limitations of the NDVI- and FCVI-based approaches

The development of saR2F highlights that incorporating TOC red and blue reflectance helps to mitigate soil effects on the R2F relationship. This insight also sheds light on the effectiveness and limitations of other soil correction approaches such as NDVI- and FCVI-based methods. Both indices involve reflectance in the visible range to empirically or semi-empirically suppress soil contributions to NIR reflectance.

Our theoretical analysis suggests that removing the single-scattering contribution of soil to R_{nir} is key to solving the black-soil problem. Both NDVI (as in NIRv) and visible reflectance (as in FCVI) achieve correction by reducing the soil-related component in R_{nir} . NIRv was initially proposed as a semi-empirical index based on its strong correlation with SIF and GPP (Badgley et al., 2017). Later studies linked NIRv to σ_F and explained its soil-correction capability by considering that NDVI approximates FVC, allowing R_{nir} scaled by NDVI to represent vegetation-only reflectance (Zeng et al., 2019).

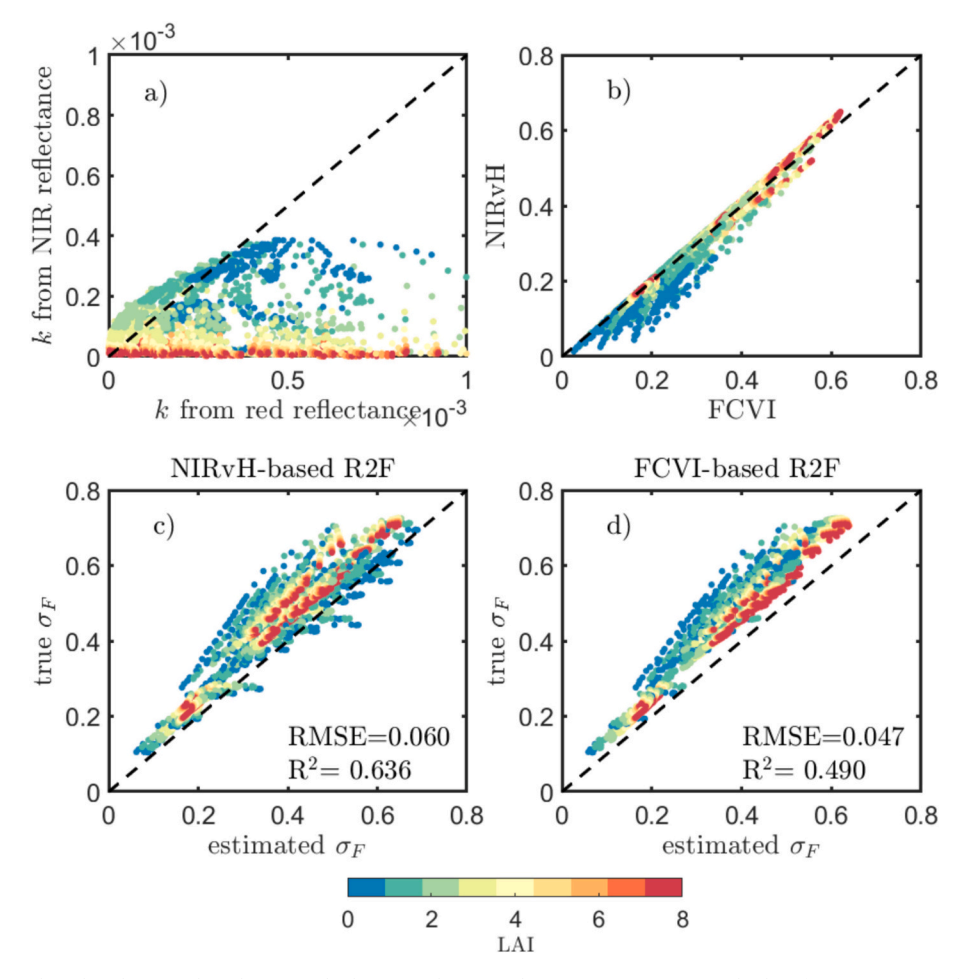


Fig. 8. Comparison of FCVI-based and NIRvH-based R2F methods, using the same dataset as in Fig. 3. (a) The key fitting parameter k in the NIRvH approach, estimated using TOC reflectance from either the red band (675–681 nm) or the NIR band (778–800 nm). (b) Direct comparison between FCVI and NIRvH values. (c–d) True and estimated σ_F estimated using NIRvH and FCVI, respectively. (For interpretation of the references to colour in this figure legend, the reader is referred to the web version of this article.)

The use of NDVI \times R_{nir} (i.e., NIRv) to estimate the NIR reflectance of 'pure' vegetation reflects the intuitive notion that vegetation contribution to the canopy signal increases with NDVI. However, this approach suffers from a fundamental logical inconsistency. For example, in a pure soil scene, the observed NDVI equals that of bare soil, which is typically greater than zero. In such cases, NIRv yields a non-zero value, even though the NIR reflectance of 'pure' vegetation should be zero by definition. Conversely, in a fully vegetated scene with no soil contribution, the observed TOC NIR reflectance should correspond directly to the NIR reflectance of pure vegetation. Yet, because canopy NDVI rarely reaches 1, NIRv underestimates the true vegetation signal. These inconsistencies highlight a key limitation of this empirical approximation. As such, this formulation may introduce bias in the retrieval of vegetation optical properties and warrants careful re-evaluation in soil correction models.

Similar to NIRv, FCVI performs reasonably well in practice, although it was originally developed under the assumption of non-reflective soil (i.e., black soil), (Figs. 3–7). Structurally, the FCVI-based and saR2F approaches are quite similar—both rely on subtracting a visible-reflectance-based component from R_{nir} . The apparent effectiveness of FCVI may be attributed to its ability to capture variations in FVC when soil reflectance remains constant. As vegetation cover increases, the TOC visible reflectance tends to approximate that of pure vegetation; conversely, in sparse canopies, it approaches that of bare soil. Thus, although FCVI does not explicitly isolate the soil contribution, its dependence on visible reflectance allows it to track FVC-related changes, partially mitigating soil background effects under certain conditions. Nevertheless, we found this is insufficient, and believe the generalizable basis for correcting soil effects on the R2F relationship in this study was necessary.

Both NIRv-based and FCVI-based methods show low RMSE, which might suggest good performance (Fig. 3). However, when comparing the estimated and true σ_F , their R² values are low, indicating that the estimates may simply cluster around the mean of the true values. This pattern implies that, despite low RMSE, these methods have weak explanatory power for variations in σ_F . This may reflect a potential issue with NDVI-based correction—while NDVI is related to soil contribution, simply multiplying R_{nir} by NDVI does not effectively remove the soil effect, and highlights the need for caution when using them in soil correction models.

It is important to note that in our soil correction, we did not adopt the NIRvH method. There are several reasons for this decision. First, NIRvH is by design intended to correct for both (1) soil single scattering and (2) soil–vegetation multiple scattering effects on R_{nir} . However, as shown in our analysis in Section 2.2, correcting the soil–vegetation multiple scattering component in R_{nir} is not appropriate, because this component also influences σ_F . Simply correcting its effect on R_{nir} does not improve the R_{nir} – σ_F relationship.

Furthermore, in our evaluation of NIRvH, we used the definition:

$$NIRvH = R_{nir} - R_{red} - k \times (\lambda_{nir} - \lambda_{red})$$
(9)

Following the recommendation of Zeng et al. (2021), we set $\lambda_{red}=678$ nm and $\lambda_{nir}=780$ nm (within the 778–800 nm range). The slope k was estimated by linearly fitting several TOC reflectance values against wavelength in either of the two spectral regions: the red band (675–681 nm) or the NIR band (778–800 nm). Our results revealed two issues: (1) The value of k differed depending on whether it was derived from the red or NIR regions (Fig. 8a). (2) Regardless of which range was used, the fitted spectral-invariant values were very small, making NIRvH essentially equivalent to FCVI in our case (Fig. 8b). Consequently, the performance of FCVI-based and NIRvH-based R2F methods is similar, although slight improvements are observed for NIRvH due to its incorporation of red reflectance.

5.3. Applications and limitations

5.3.1. Applications of the saR2F relationship

The relationship between R_{nir} and σ_F enables three main applications: (1) correcting directional effects on SIF using reflectance, (2) estimating total emitted SIF from directional SIF and reflectance, and (3) converting SIF across spatial scales. These capabilities are essential for linking remote sensing observations to photosynthetic processes such as GPP and LUE.

Since the R2F concept was first proposed in 2018, it has been adopted in a growing number of studies across various spatial scales, including site-level experiments, UAV-based observations, and global satellite retrievals (Mohammed et al., 2019a). However, in many of these applications, soil background effects have been treated in a simplified manner. Some studies have ignored soil contributions, while others have excluded low-vegetation-cover pixels to avoid contamination (Zhang et al., 2019). Alternatively, NDVI- or FCVI-based correction methods have been employed to mitigate soil influences (Bendig et al., 2025; Merrick et al., 2021). This study provides a more systematic analysis of the impact of soil on both R_{nir} and σ_F . As demonstrated in Appendix B, the influence of soil on σ_F can be substantial, although part of this effect is offset by the soil's contribution to R_{vir} . This finding challenges the assumption that soil has little to no effect on SIF and updates our understanding of the factors influencing TOC fluorescence signals (Zeng et al., 2019). By explicitly accounting for soil effects, the saR2F framework provides a more robust and physically interpretable approach for a range of applications-including angular correction, estimation of total emitted SIF (F_{tot}), and improved retrievals of photosynthetic activity such as GPP. As such, the methodology presented here offers a promising pathway to enhance both the accuracy and applicability of existing and future SIF-related studies.

Soil correction is particularly important for the remote sensing of vegetation physiological signals, as soil typically acts as a confounding factor. The soil correction method proposed here builds upon the earlier work of Yang et al. (2025), where it was systematically evaluated and shown to be applicable to other reflectance-based indices, such as the Photochemical Reflectance Index (PRI) (Yang, 2024; Yang, 2022). Whether using SIF or PRI for assessing vegetation physiology, soil correction can facilitate more reliable downscaling from canopy- to leaflevel signals, thereby improving the monitoring of physiological processes.

5.3.2. Limitations of the theoretical development and evaluation

Despite its advantages, the saR2F relationship also has limitations that should be considered when applying it to real-world scenarios. First, the theoretical foundation of saR2F is based on a two-component canopy composed solely of green leaves and underlying soil. However, natural vegetation often includes non-photosynthetic components such as woody material (branches, stems) or senescent leaves, which contribute to TOC reflectance. In such three-component systems, TOC reflectance is contributed not only from soil and green foliage but also from additional scattering and absorption by these non-photosynthetic elements. The direct reflectance by the non-photosynthetic parts needs to be subtracted besides the soil effects.

In addition to the structural complexity, the soil correction method implemented in saR2F relies on several simplifying assumptions. For instance, it assumes that red and blue reflectance of green leaves are close to zero, and that soil reflectance between 400 and 1000 nm varies approximately linearly with wavelength. While these assumptions are generally supported by field and simulated data, there are situations—such as high-sand-content soils, litter-covered surfaces, or atypical vegetation types—where they may break down, potentially compromising the accuracy of the correction.

Additionally, although the saR2F framework improves the physical interpretability and robustness of σ_F estimation, it still requires knowledge of canopy interceptance (i_0), a structural variable that is difficult to

obtain directly from satellite observations. Although i_0 can be approximated using LAI and clumping index, uncertainties in these parameters may propagate into σ_F estimates. Therefore, future work should explore integrating saR2F with structural parameter retrieval methods, such as 3D radiative transfer models or machine-learning-based approaches trained on high-resolution datasets.

The saR2F formulation in this study is based on narrowband reflectance at 438 nm and 675 nm, corresponding to regions of strong chlorophyll absorption. While this spectral specificity enhances the method's sensitivity to vegetation optical properties, it also raises questions regarding its applicability to multispectral observations, where only broader bands (e.g., MODIS, Landsat, Sentinel-3) are available. According to Yang et al. (2025), we expect that the adaptation of our soil correction approach to broadband data remains effective in reducing soil background effects, although its performance varied depending on the sensor band configuration and bandwidth. Substituting the narrow bands in saR2F with available broadband red and blue channels can still yield meaningful improvements over conventional indices, but the magnitude of the benefit depends on the specific spectral coverage and overlap with absorption features. However, the use of blue reflectance (~438 nm) also introduces potential challenges for satellite-based applications. Blue wavelengths are more susceptible to atmospheric effects, particularly aerosol scattering, which can increase uncertainties in surface reflectance retrieval if not properly corrected. This sensitivity may reduce the robustness of saR2F in regions or seasons with high aerosol loading, such as dust-prone areas or during biomass burning events. Therefore, applying saR2F at large scales requires robust atmospheric correction strategies to mitigate these effects. A comprehensive evaluation of broadband-adapted saR2F across multiple platforms, especially using actual satellite data, is beyond the scope of the present study but represents an important avenue for future work.

Finally, our evaluation of the correction methods is also subject to several limitations. In the context of SIF studies, the inability to directly measure σ_F and F_{tot} makes it particularly challenging to assess the accuracy of proposed correction schemes. For example, in our field dataset, soil reflectance and canopy structure remained nearly constant, and only the viewing azimuth was varied. Under these controlled conditions, the benefits of soil correction can be observed; however, the differences among the saR2F method, FCVI-based correction, and NDVI-based approaches remain relatively subtle (Fig. 7). In contrast, under simulated scenarios where both viewing geometry and LAI are allowed to vary, the distinctions among these methods become much more pronounced (Figs. 5 and 6). Nevertheless, model validation is inevitably influenced by the design of the experimental or simulated scenarios, which may unintentionally bias the outcome in favor of a particular method. Therefore, we argue that rigorous theoretical derivation is indispensable for advancing SIF correction methodologies. Compared to empirical fitting alone, a clear physical foundation offers a more robust and generalizable basis for methodological development.

6. Conclusions

We revisited the reflectance-to-fluorescence (R2F) relationship and proposed an improved soil-adjusted version (saR2F) to explicitly account for soil effects. While the original R2F framework offers a valuable

theoretical basis for interpreting canopy-level SIF signals, its assumption of a non-reflective soil limits its applicability—particularly in sparse canopies where soil contributions are non-negligible. We show while soil-vegetation multiple scattering affects both NIR reflectance and the scattering coefficient of emitted SIF, it does so in a comparable manner, and thus does not fundamentally disrupt the applicability of the original R2F relationship. In contrast, the dominant source of bias in sparse canopies arises from the extra contribution of soil single scattering to NIR reflectance, which has no counterpart in the scattering coefficient of emitted SIF.

The proposed saR2F formulation incorporates TOC red and blue reflectance to estimate and remove the direct soil contribution, enabling more accurate estimation of the SIF scattering coefficient. Our results show that saR2F significantly improves the consistency of reflectance–SIF relationships across different canopy structures and viewing geometries. Compared to existing NDVI- or FCVI-based correction approaches, saR2F offers a more physically plausible and interpretable solution that can be applied to angular correction, total SIF estimation, and photosynthetic monitoring. Overall, the saR2F approach provides a unified, scalable, and physically robust tool for improving the accuracy of SIF-based vegetation physiological assessments—from the leaf to the satellite scale. This work lays the groundwork for more reliable generation and interpretation of next-generation SIF remote sensing products.

CRediT authorship contribution statement

Peiqi Yang: Writing – review & editing, Writing – original draft, Visualization, Resources, Project administration, Methodology, Investigation, Funding acquisition, Formal analysis, Data curation, Conceptualization. Zhigang Liu: Writing – review & editing, Methodology, Investigation, Data curation. Dalei Han: Writing – review & editing, Investigation. Runfei Zhang: Writing – review & editing, Investigation. Bastian Siegmann: Writing – review & editing, Investigation. Jing Liu: Writing – review & editing, Investigation. Huarong Zhao: Writing – review & editing, Investigation. Uwe Rascher: Writing – review & editing, Investigation. Jing M. Chen: Writing – review & editing, Investigation. Christiaan van der Tol: Writing – review & editing, Methodology, Investigation, Conceptualization.

Declaration of competing interest

The authors declare that they have no known competing financial interests or personal relationships that could have appeared to influence the work reported in this paper.

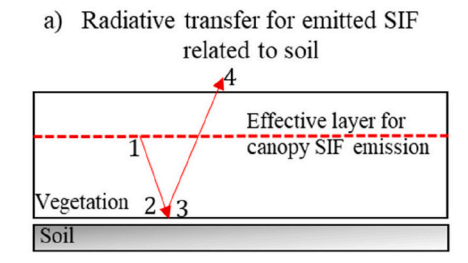
Acknowledgements

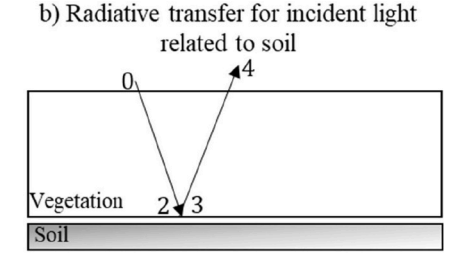
This research was supported by the National Natural Science Foundation of China (NSFC) under grant 42471421 and the Jiangsu Natural Science Foundation (No. BK20241884). This work has partially been funded by the Deutsche Forschungsgemeinschaft (DFG, German Research Foundation) under Germany's Excellence Strategy – EXC 2070 – 390732324. Data can be shared upon reasonable request and under data use agreements.

Appendix A. Analysis of soil effects on R2F using the four-stream theory

In Section 2, we narrow down the soil effects on the R2F relationship to the single scattering of soil to R_{nir} with a conceptual figure. In what follows, we present the specific derivations by using the four-stream radiative transfer theory.

The four-stream theory considers four types of radiative fluxes: direct solar flux, diffuse downward flux, diffuse upward flux, direct flux in the direction of observer (Verhoef, 1984). We follow the notation in the four-stream theory for the transmittances of a vegetation canopy and examine the effects of soil on canopy SIF scattering and reflectance.





Region	Relative intensity (SIF)
1 (source)	1
2	$ au_{dd}^f$
3	$ au_{dd}^f R_{nir}^s$
4	$ au_{dd}^f R_{nir}^s au_{do}$

Region	Relative intensity (NIR Refl.)
0 (source)	1
2	$ au_{ss} + au_{sd}$
3	$(\tau_{ss} + \tau_{sd}) R_{nir}^s$
4	$(\tau_{ss}\tau_{oo}+\tau_{sd}\tau_{do})R^s_{nir}$

Fig. A1. Diagram for the radiative transfer of incident radiation and emitted SIF.

For the scattering coefficient of far-red SIF σ_F , the enhancement by the soil is given as

$$\delta_{\sigma} = \sigma_{\rm F}^1 - \sigma_{\rm F}^0 = \tau_{ds}^I R_{nir}^{\rm s} \tau_{do} \tag{A1a}$$

where the superscript '1' is introduced to denote the scattering coefficient for non-black-soil canopies. The enhancement δ_{σ} denotes the fraction of the total emitted SIF that is scattered by soil and detected by the sensor. It is determined by the downward transmittance of the total emitted SIF τ_{dd}^f , soil reflectance R_{nir}^s and upward transmittance τ_{do} of the reflected SIF by soil. Canopy transmittance τ_{do} is the diffuse-directional transmittance of the canopy. The subscripts 'd' and 'o' denote diffuse incoming radiation and outgoing radiation in the observer's direction, respectively. R_{nir}^s is the soil reflectance at the NIR region. The transmittance τ_{dd}^f is the effective downward transmittance for the total emitted SIF by all leaves. It differs from τ_{dd} by the position of the radiative source (i.e., top of canopy for τ_{dd}^f , inside the canopy for τ_{dd}^f).

While for NIR reflectance, the enhancement by the soil is given as

$$\delta_{Rnir} = R_{nir}^1 - R_{nir}^0 = \tau_{ss} R_{nir}^s \tau_{oo} + \tau_{sd} R_{nir}^s \tau_{do} \tag{A2}$$

where τ_{ss} and τ_{sd} denote canopy transmittance for the incoming solar beam. Note we assume the soil reflectance is isotropic. The magnitudes of $\tau_{ss}\tau_{oo}$ and $\tau_{sd}\tau_{do}$ depend on the number of scatters (i.e., leaves) in the canopy: $\tau_{ss}\tau_{oo}$ decreases with the increasing LAI, while $\tau_{sd}\tau_{do}$ increases with LAI.

According to the enhancement on canopy reflectance and SIF scattering shown in Eq. A1 and Eq. A2, we obtain the relationship between them for non-black-soil canopies by revising Eq. 2.

$$\sigma_{\rm F}^1 = \frac{R_{nir}^1}{i_0} + \delta_{R2F}$$
 (A3)

By introducing Eq. A1 and Eq. A2 into Eq. A3, and we obtain a correction factor δ_{R2F} for the R2F relationship

$$\delta_{R2F} = \sigma_{\rm F}^0 + \delta_{\sigma} - \frac{R_{nir}^0 + \delta_{Rnir}}{i_0} \tag{A4}$$

Hence, knowing from Eq. 2 that $\sigma_F^0 - \frac{R_{nir}^0}{i_0} = 0$, the correction factor for soil effects is

$$\delta_{R2F} = \delta_{\sigma} - \frac{\delta_{Rnir}}{i_0} = \left(\tau_{dd}^f \tau_{do} - \frac{\tau_{ss} \tau_{oo} + \tau_{sd} \tau_{do}}{i_0}\right) R_{nir}^s \tag{A5}$$

The transmittances in Eq. A5 are unknown. Nevertheless, we conduct some empirical analysis to the soil correction factor. For dense canopies, the largeest part of incoming PAR is absorbed by leaves at the upper layer, and by extension, the effective downward transmittance of canopy SIF τ_{dd}^f is close to τ_{sd} . Moreover, i_0 is close to unity and the transmittances τ_{ss} and τ_{oo} are close to zero due to limited gaps. Therefore, $\tau_{dd}^f \tau_{do}$ is close to $\frac{\tau_{sd}\tau_{do}}{i_0}$, and $\frac{\tau_{ss}\tau_{oo}}{i_0}$ is small. As a result, δ_{R2F} can be neglected. This implies that the soil effects in dense canopies do not significantly alter the relationship between R_{nir} and σ_F .

For sparse canopies, direct transmittances for the direct incident light $\tau_{ss}\tau_{oo}$ are large due to limited number of leaves for intercepting the light. In contrast, the transmittances for diffuse incoming to direct outgoing radiation, and direct incoming to diffuse outgoing (i.e., τ_{do} and τ_{sd}) are small, since the number of leaves to scatter the direct incident light to diffuse light or vice versa is limited. Therefore, we expect that $\tau_{dd}^f \tau_{do} - \frac{\tau_{sd}\tau_{do}}{i_0}$ is much smaller than $\frac{\tau_{sd}\tau_{oo}}{i_0}$. Hence, δ_{R2F} is largely determined by $\frac{\tau_{sd}\tau_{oo}}{i_0}R_s^{nir}$. This approximation is also intuitive and rational. The contribution of soil to canopy reflectance is mainly denominated by the single scattering of soil, $\tau_{ss}\tau_{oo}R_s^{nir}$, for sparse canopies. The contribution of multiple scattering to TOC SIF and reflectance is similar.

Thus, we can estimate the canopy scattering of far-red SIF for non-black soil cases as:

$$\sigma_{\rm F}^1 = \frac{R_{nir}^1 - \tau_{ss} \tau_{oo} R_{nir}^s}{i_o} \tag{A6a}$$

$$\sigma_{\rm F}^1 = \frac{R_{nir}^1 - P_{soil}^{soil} R_{nir}^s}{i_0} \tag{A6b}$$

Appendix B. Analysis of the soil effects on R2F using simulated datasets

The replacement of black soil with non-black soil leads to higher R_{nir} and σ_F (Fig. B1). The differences are substantially smaller for the canopies with high LAI values. For the canopies with an LAI greater than 3, the difference in R_{nir} of black-soil and non-black-soil scenarios generally remains below 0.06 (red bars in Fig. B1a), and the difference in σ_F is less than 0.05 (red bars in Fig. B1b). In these scenarios, the variation is negligible, with around 80 % of scenarios displaying differences below 0.01. In contrast, the differences are more pronounced for canopies with an LAI below 3. In such cases, the disparity in R_{nir} reaches up to 0.3 between black-soil and non-black-soil scenarios, and the differences in σ_F are as high as 0.2.

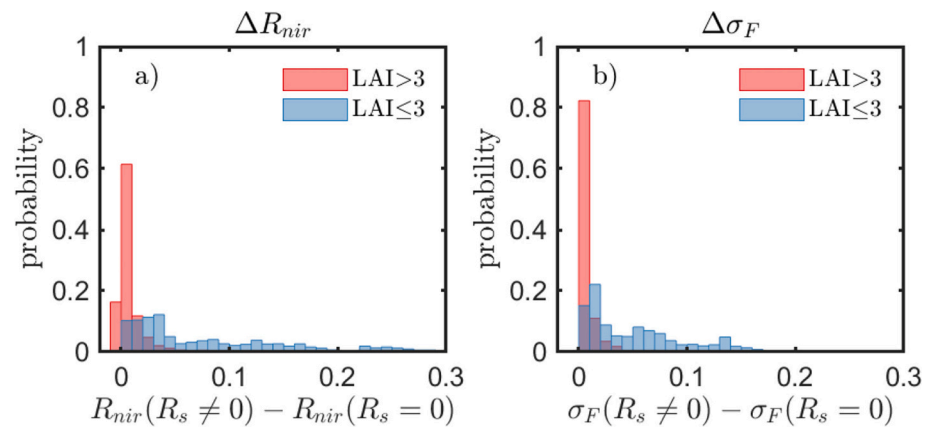


Fig. B1. The effects of soil on NIR reflectance (R_{nir} , a) and scattering coefficient of far-red SIF (σ_F , b) for dense (LAI> 3) and sparse (LAI \le 3) canopies. Shown the distributions of the probability of the difference between non-black-soil canopies ($R_s \ne 0$) and the corresponding black-soil canopies ($R_s = 0$). (For interpretation of the references to colour in this figure legend, the reader is referred to the web version of this article.)

The impacts of LAI on the difference in R_{nir} and σ_F of black-soil and non-black-soil scenarios are presented in Fig. B2. When LAI exceeds 3, the discrepancy in R_{nir} is less than 0.05, and the difference is even smaller for σ_F . The canopies with an LAI of 8 exhibit minimal effects from the soil on both R_{nir} and σ_F . In contrast, the canopies with an LAI of 0.5 display a mean difference of 0.14 in R_{nir} and a mean difference of 0.06 in σ_F . The variability in differences for the same LAI are attributed to variations in leaf biophysical properties, soil reflectance, leaf angle distribution (LAD), and sun-observer geometry.

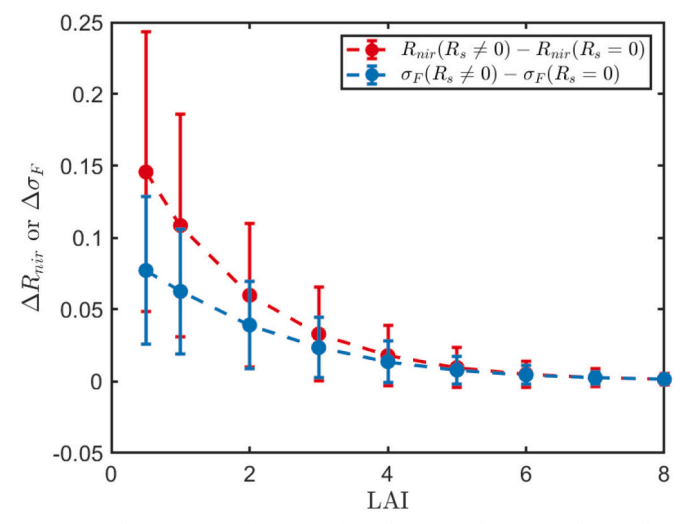


Fig. B2. The effects of soil on NIR reflectance (R_{nir}) and scattering coefficient of far-red SIF (σ_F) changing with LAI. Shown the mean values and standard deviations of the differences between non-black-soil canopies ($R_s \neq 0$) and the corresponding black-soil canopies ($R_s = 0$) for various scenarios. (For interpretation of the references to colour in this figure legend, the reader is referred to the web version of this article.)

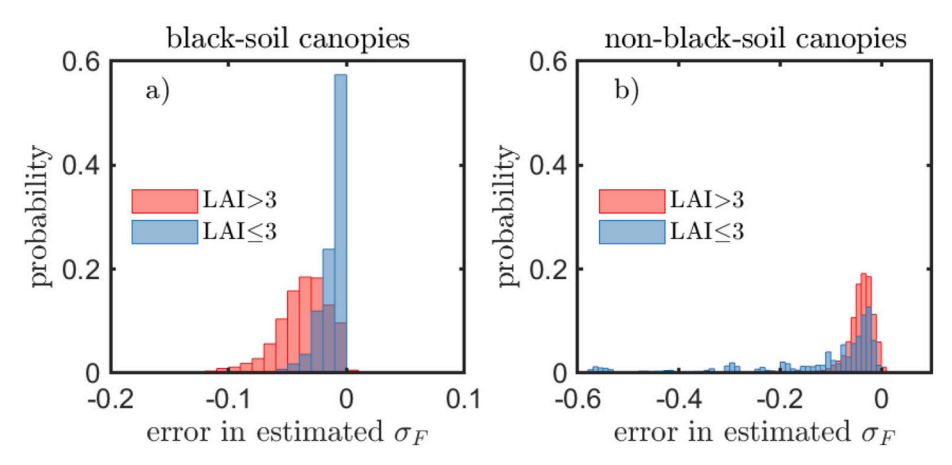


Fig. B3. The error in the original R2F relationship expressed as the difference between the true and estimated scattering coefficient of far-red SIF (σ_F), $\delta_{R2F} = \sigma_F - R_{nir}/i_0$. Shown the distributions of the probability of the error for the black-soil canopies ($R_s = 0$, a) and non-black-soil canopies ($R_s \neq 0$, b). (For interpretation of the references to colour in this figure legend, the reader is referred to the web version of this article.)

The original R2F relationship provides reasonably accurate estimation of σ_F for the black soil canopies (depicted in Fig. B3a), but the performance in the non-black-soil canopies is unacceptable when the canopies LAI is less than 3 (depicted in Fig. B3b). In the black-soil canopies, the errors span from -0.1 to 0.01. In over 50 % of the scenarios, the errors are within the narrow range of less than 0.05. Furthermore, the error distributions exhibit a similar pattern irrespective of whether the canopies possess large or small LAI. In contrast, in the non-black-soil canopies, the error distributions exhibit a broader spectrum, and is strongly affected by canopy LAI (Fig. B3b). When the LAI of the canopies is less than 3, the errors are as large as 0.6. However, when the LAI exceeds 3, the errors vary from -0.1 to 0, which is similar to the range for the black-soil scenarios.

The original R2F relationship provides accurate estimation of σ_F across different canopy LAI under the black soil condition (Fig. B4). The error remains relatively stable, with the mean value for a specific LAI less than 0.05. In contrast, for non-black-soil scenarios, there is a notable decrease in error as the canopy LAI increases. When the canopy LAI surpasses 3, the error becomes comparable to that observed in black-soil scenarios. However, for the canopies with a low LAI of 0.5, the mean error is 0.4. For these canopies, there are considerable variations in the errors.

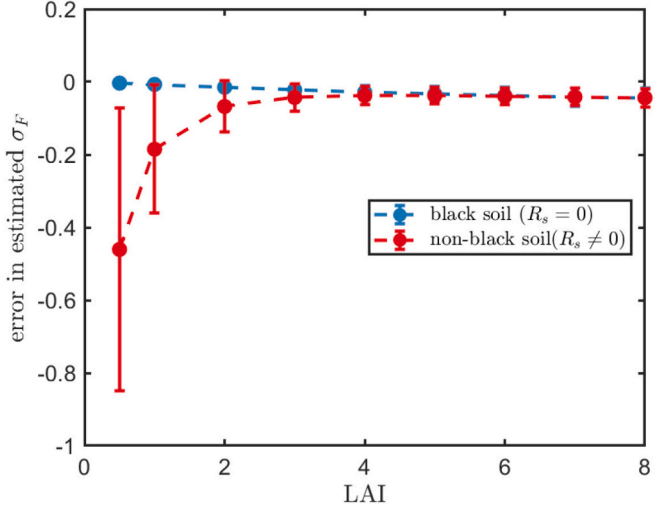


Fig. B4. The error in the estimated $σ_F$ by using the original R2F relationship for varying LAI for the black-soil canopies ($R_s = 0$) and the non-black-soil canopies ($R_s \neq 0$). The error is expressed as the difference between the true ($σ_F$) and estimate (R_{nir}/i_0) scattering coefficient of far-red SIF, $δ_{R2F} = σ_F - R_{nir}/i_0$. (For interpretation of the references to colour in this figure legend, the reader is referred to the web version of this article.)

Data availability

Data will be made available on request.

References

Badgley, G., Field, C.B., Berry, J.A., 2017. Canopy near-infrared reflectance and terrestrial photosynthesis. Sci. Adv. 3, 1–6. https://doi.org/10.1126/ sciadv.1602244.

Baker, N.R., 2008. Chlorophyll fluorescence: a probe of photosynthesis in vivo. Annu. Rev. Plant Biol. 59, 89–113. https://doi.org/10.1146/annurev. arriant 50.032607.092759

Bendig, J., Malenovský, Z., Siegmann, B., Krämer, J., Rascher, U., 2025. Comparing methods for solar-induced fluorescence efficiency estimation using radiative transfer modelling and airborne diurnal measurements of barley crops. Remote Sens. Environ. 317, 114521, https://doi.org/10.1016/i.rse.2024.114521.

Cogliati, S., Celesti, M., Cesana, I., Miglietta, F., Genesio, L., Julitta, T., Schuettemeyer, D., Drusch, M., Rascher, U., Jurado, P., Colombo, R., 2019. A spectral fitting algorithm to retrieve the fluorescence spectrum from canopy radiance. Remote Sens 11. https://doi.org/10.3390/rs11161840.

Hao, D., Asrar, G.R., Zeng, Y., Yang, X., Li, X., Xiao, J., Guan, K., Wen, J., Xiao, Q., Berry, J.A., Chen, M., 2021a. Potential of hotspot solar-induced chlorophyll fluorescence for better tracking terrestrial photosynthesis. Glob. Chang. Biol. 27, 2144–2158. https://doi.org/10.1111/ecb.15554.

Hao, D., Zeng, Y., Qiu, H., Biriukova, K., Celesti, M., Migliavacca, M., Rossini, M., Asrar, G.R., Chen, M., 2021b. Practical approaches for normalizing directional solar-induced fluorescence to a standard viewing geometry. Remote Sens. Environ. 255, 112171. https://doi.org/10.1016/j.rse.2020.112171.

He, L., Chen, J.M., Liu, J., Mo, G., Joiner, J., 2017. Angular normalization of GOME-2 Sun-induced chlorophyll fluorescence observation as a better proxy of vegetation

- productivity. Geophys. Res. Lett. 44, 5691–5699. https://doi.org/10.1002/
- Hinojo-Hinojo, C., Goulden, M.L., 2020. Plant traits help explain the tight relationship between vegetation indices and gross primary production. Remote Sens 12, 1405.
- Joiner, J., Yoshida, Y., Köhler, P., Campbell, P., Frankenberg, C., van der Tol, C., Yang, P., Parazoo, N., Guanter, L., Sun, Y., 2020. Systematic orbital geometrydependent variations in satellite solar-induced fluorescence (SIF) retrievals. Remote Sens 12. https://doi.org/10.3390/RS12152346.
- Krämer, J., Siegmann, B., Castro, A.O., Muller, O., Pude, R., Döring, T., Rascher, U., 2025. Downscaling the full-spectrum solar-induced fluorescence emission signal of a mixed crop canopy to the photosystem level using the hybrid approach. Remote Sens. Environ. 324, 114739.
- Li, X., Lu, H., Yu, L., Yang, K., 2018. Comparison of the spatial characteristics of four remotely sensed leaf area index products over China: direct validation and relative uncertainties. Remote Sens 10. https://doi.org/10.3390/rs10010148.
- Liu, L., Liu, X., Wang, Z., Zhang, B., 2016. Measurement and analysis of bidirectional SIF emissions in wheat canopies. IEEE Trans. Geosci. Remote Sens. 54, 2640–2651. https://doi.org/10.1109/TGRS.2015.2504089.
- Liu, X., Guanter, L., Liu, L., Damm, A., Malenovský, Z., Rascher, U., Peng, D., Du, S., Gastellu-Etchegorry, J.P., 2019. Downscaling of solar-induced chlorophyll fluorescence from canopy level to photosystem level using a random forest model. Remote Sens. Environ. 231, 110772. https://doi.org/10.1016/j.rse.2018.05.035.
- Lu, X., Liu, Z., Zhao, F., Tang, J., 2020. Comparison of total emitted solar-induced chlorophyll fluorescence (SIF) and top-of-canopy (TOC) SIF in estimating photosynthesis. Remote Sens. Environ. 251, 112083. https://doi.org/10.1016/j. rse.2020.112083.
- Merrick, T., Pau, S., Detto, M., Broadbent, E.N., Bohlman, S.A., Still, C.J., Almeyda Zambrano, A.M., 2021. Unveiling spatial and temporal heterogeneity of a tropical forest canopy using high-resolution NIRv, FCVI, and NIRvrad from UAS observations. Biogeosciences 18, 6077–6091. https://doi.org/10.5194/bg-18-6077-2021.
- Mohammed, G.H., Colombo, R., Middleton, E.M., Rascher, U., 2019a. Remote sensing of solar-induced chlorophyll fluorescence (SIF) in vegetation: 50 years of progress. Remote Sens. Environ. 231, 111177. https://doi.org/10.1016/j.rse.2019.04.030.
- Mohammed, G.H., Colombo, R., Middleton, E.M., Rascher, U., van der Tol, C., Nedbal, L., Goulas, Y., Pérez-Priego, O., Damm, A., Meroni, M., Joiner, J., Cogliati, S., Verhoef, W., Malenovský, Z., Gastellu-Etchegorry, J.P., Miller, J.R., Guanter, L., Moreno, J., Moya, I., Berry, J.A., Frankenberg, C., Zarco-Tejada, P.J., 2019b. Remote sensing of solar-induced chlorophyll fluorescence (SIF) in vegetation: 50 years of progress. Remote Sens. Environ. 231, 111177. https://doi.org/10.1016/j. rse.2019.04.030.
- Porcar-Castell, A., Tyystjärvi, E., Atherton, J., Van Der Tol, C., Flexas, J., Pfündel, E.E., Moreno, J., Frankenberg, C., Berry, J.A., 2014. Linking chlorophyll a fluorescence to photosynthesis for remote sensing applications: mechanisms and challenges. J. Exp. Bot. 65, 4065–4095. https://doi.org/10.1093/jxb/eru191.
- Siegmann, B., Cendrero-Mateo, M.P., Cogliati, S., Damm, A., Gamon, J., Herrera, D., Jedmowski, C., Junker-Frohn, L.V., Kraska, T., Muller, O., Rademske, P., van der Tol, C., Quiros-Vargas, J., Yang, P., Rascher, U., 2021. Downscaling of far-red solar-induced chlorophyll fluorescence of different crops from canopy to leaf level using a diurnal data set acquired by the airborne imaging spectrometer HyPlant. Remote Sens. Environ. 264, 112609. https://doi.org/10.1016/j.rse.2021.112609.
- Smolander, S., Stenberg, P., 2005. Simple parameterizations of the radiation budget of uniform broadleaved and coniferous canopies. Remote Sens. Environ. 94, 355–363. https://doi.org/10.1016/j.rse.2004.10.010.
- Stenberg, P., Manninen, T., 2015. The effect of clumping on canopy scattering and its directional properties: a model simulation using spectral invariants. Int. J. Remote Sens. 36, 5178–5191. https://doi.org/10.1080/01431161.2015.1049383.

- Stenberg, P., Möttus, M., Rautiainen, M., 2016. Photon recollision probability in modelling the radiation regime of canopies - a review. Remote Sens. Environ. https://doi.org/10.1016/j.rse.2016.05.013.
- Van Der Tol, C., Verhoef, W., Timmermans, J., Verhoef, A., Su, Z., 2009. An integrated model of soil-canopy spectral radiances, photosynthesis, fluorescence, temperature and energy balance. Biogeosciences 6, 3109–3129. https://doi.org/10.5194/bg-6-3109-3109
- Verhoef, W., 1984. Light scattering by leaf layers with application to canopy reflectance modeling: the SAIL model. Remote Sens. Environ. 16, 125–141. https://doi.org/ 10.1016/0034-4257(84)90057-9.
- Vilfan, N., Van der Tol, C., Yang, P., Wyber, R., Malenovský, Z., Robinson, S.A., Verhoef, W., 2018. Extending Fluspect to simulate xanthophyll driven leaf reflectance dynamics. Remote Sens. Environ. 211, 345–356. https://doi.org/ 10.1016/j.rse.2018.04.012.
- Wan, L., Ryu, Y., Dechant, B., Lee, J., Zhong, Z., Feng, H., 2024. Improving retrieval of leaf chlorophyll content from Sentinel-2 and Landsat-7/8 imagery by correcting for canopy structural effects. Remote Sens. Environ. 304, 114048.
- Yang, P., 2022. Exploring the interrelated effects of soil background, canopy structure and sun-observer geometry on canopy photochemical reflectance index. Remote Sens. Environ. 279, 113133. https://doi.org/10.1016/j.rse.2022.113133.
- Yang, P., 2024. Downscaling canopy photochemical reflectance index to leaf level by correcting for the soil effects. Remote Sens. Environ. 311, 114250. https://doi.org/ 10.1016/j.rse.2024.114250.
- Yang, P., van der Tol, C., 2018. Linking canopy scattering of far-red sun-induced chlorophyll fluorescence with reflectance. Remote Sens. Environ. 209, 456–467. https://doi.org/10.1016/j.rse.2018.02.029.
- Yang, P., van der Tol, C., Campbell, P.K.E., Middleton, E.M., 2020. Fluorescence correction vegetation index (FCVI): a physically based reflectance index to separate physiological and non-physiological information in far-red sun-induced chlorophyll fluorescence. Remote Sens. Environ. 240, 111676. https://doi.org/10.1016/j. rse.2020.111676.
- Yang, P., Prikaziuk, E., Verhoef, W., Van Der Tol, C., 2021. SCOPE 2.0: a model to simulate vegetated land surface fluxes and satellite signals. Geosci. Model Dev. 14, 4697–4712. https://doi.org/10.5194/gmd-14-4697-2021.
- Yang, P., Van Tol, C., Der, Liu J., Liu, Z., 2025. Separation of the Direct Reflection of Soil from Canopy Spectral Reflectance. Remote Sens, Environ, p. 316.
- Zeng, Y., Badgley, G., Dechant, B., Ryu, Y., Chen, M., Berry, J.A., 2019. A practical approach for estimating the escape ratio of near-infrared solar-induced chlorophyll fluorescence. Remote Sens. Environ. 232, 111209. https://doi.org/10.1016/j.rse.2019.05.028.
- Zeng, Y., Hao, D., Badgley, G., Damm, A., Rascher, U., Ryu, Y., Johnson, J., Krieger, V., Wu, S., Qiu, H., Liu, Y., Berry, J.A., Chen, M., 2021. Estimating near-infrared reflectance of vegetation from hyperspectral data. Remote Sens. Environ. 267, 112723. https://doi.org/10.1016/j.rse.2021.112723.
- Zhang, Z., Chen, J.M., Guanter, L., He, L., Zhang, Y., 2019. From canopy-leaving to Total canopy far-red fluorescence emission for remote sensing of photosynthesis: first results from TROPOMI. Geophys. Res. Lett. 46, 12030–12040. https://doi.org/ 10.1029/2019GL084832
- Zhang, Z., Zhang, Y., Porcar-Castell, A., Joiner, J., Guanter, L., Yang, X., Migliavacca, M., Ju, W., Sun, Z., Chen, S., Martini, D., Zhang, Q., Li, Z., Cleverly, J., Wang, H., Goulas, Y., 2020a. Reduction of structural impacts and distinction of photosynthetic pathways in a global estimation of GPP from space-borne solar-induced chlorophyll fluorescence. Remote Sens. Environ. 240, 111722. https://doi.org/10.1016/j. rse.2020.111722.
- Zhang, Z., Zhang, Yongguang, Zhang, Yao, Gobron, N., Frankenberg, C., Wang, S., Li, Z., 2020b. The potential of satellite FPAR product for GPP estimation: an indirect evaluation using solar-induced chlorophyll fl uorescence. Remote Sens. Environ. 240, 111686. https://doi.org/10.1016/j.rse.2020.111686.